THESIS
Spectrum Analysis of the Conductance of Open Quantum Dots

Keita Sasada
Department of Physics, University of Tokyo
Komaba, Meguro, Tokyo 153-8505

December 19, 2007

Abstract

A purpose of the present thesis is to analyze the conductance of an N-level quantum dot with multiple semi-infinite leads. First, we obtain a simple conductance formula that contains only the local density of states of the discrete eigenstates and the local density of states of the leads, where the discrete eigenstates consist of the bound states, the resonant states and the anti-resonant states.

Second, by using the conductance formula, we show that the symmetry of the conductance peak arises from the interference between the resonant states as well as between a resonant state and a bound state.

Finally, we *derive* the Fano parameter from the local density of states of the discrete eigenvalues. In previous studies in the literature, the Fano parameter has been used only phenomenologically to describe the shape of an asymmetric conductance peak. We show that the Fano asymmetric peak can be understood in terms of the interference between resonant states as well as between a resonant state and a bound state. We thereby relate the Fano parameter to the local density of states of the discrete eigenvalues.

Contents

Acknowledgements

I would like to express my gratitude to Professor Naomichi Hatano for his helpful suggestions and discussions. I am grateful to Dr. Manabu Machida for his advice, Dr. Akinori Nishino for many discussions, Dr. Takashi Imamura for useful suggestions, Dr. Tomio Petrosky for suggestion and advice and Dr. Gonzalo Ordonez for useful discussion. I also acknowledge helps from Mr. Yuichi Nakamura, Mr. Shiho Akagawa , Ms. Mari Matsuo and Mr. Naoya Sato.

Chapter 1

Introduction

The electron conduction in nano-scale systems has been studied extensively in recent years [1]. The resonant transport is one of its interesting phenomena, where resonant states affect the conductance in its ballistic transport regime. The resonant transport is an intrinsic feature of general open systems. The quantum mechanics of the open system, however, has not been developed so much as applicable to the computation of the conductance of nano-scale systems. We here propose a conductance formula of a class of open quantum dot systems by using the discrete eigenstates.

We are particularly interested in an asymmetric conductance peak, namely the Fano effect [2]. It is a conventional understanding that the Fano effect arises from the coupling of continuous states in the leads and discrete states in the device [3, 4]. In contrast, we here stress the importance of the interference between two of resonant states as well as between a resonant state and a bound state when we consider the Fano conductance peak. We show [5] that the complex eigenvalues of the resonant states of the whole system, the quantum dot with the leads, form the asymmetric conductance peak.

The present thesis is organized as follows. In Chap. 2, we derive a conductance formula consisted only of the local density of states of the discrete eigenstates and the local density of states of the leads. In Chap. 3, we suggest that the symmetry of the conductance peak arises from the interference between the resonant states as well as between a resonant state and a bound state. In Chap. 4, we calculate the conductance and discrete eigenvalues of the C_{60} with two semi-infinite leads attached.

Chapter 2

Spectrum analysis of an open quantum N-level dot

In the present chapter, we discuss an N-level extension of the Friedrichs model. We derive a remarkably simple conductance formula for the model. The formula contains only the local density of states of the discrete eigenstates and the local density of states of the leads.

2.1 Open quantum N-level dot

We consider a one-body Hamiltonian of an N-level dot with semi-infinite leads $\{\alpha\}$ attached to it (Fig. 2.1);

$$H = H_{\rm d} + \sum_{\alpha} \left(H_{\alpha} + H_{{\rm d},\alpha} \right) \tag{2.1}$$

with

$$\left\{ \begin{array}{lcl} H_{\rm d} & \equiv & \displaystyle\sum_{i=0}^{N-1} \epsilon_i |d_i\rangle\langle d_i| - \sum_{0 \leqslant i < j \leqslant N-1} \left(v_{ij} |d_i\rangle\langle d_j| + {\rm h.c.} \right), \\ H_{\alpha} & \equiv & \displaystyle -t \sum_{x_\alpha=0}^{\infty} \left(|x_\alpha + 1\rangle\langle x_\alpha| + {\rm h.c.} \right), \\ H_{{\rm d},\alpha} & \equiv & -t_\alpha \left(|x_\alpha = 0\rangle\langle d_0| + {\rm h.c.} \right). \end{array} \right. \tag{2.2}$$

The Hamiltonian $H_{\rm d}$ is the one of the N-level dot, while H_α is the tight-binding Hamiltonian of the one-dimensional semi-infinite lead α and $H_{{\rm d},\alpha}$ is

the hopping between a site d_0 on the central dot and the end site $x_\alpha = 0$ of the lead α. Note that all the leads are attached to the single site d_0 of the dot; this is due to a technical requirement that appears below. The system is an N-level extension of the Friedrichs model [6, 7, 8, 9].

By using the Fourier transformation and its inverse

$$|k,\alpha\rangle = \sum_{x_\alpha=0}^{\infty} e^{ikx_\alpha}|x_\alpha\rangle \qquad \text{for } -\pi < k \leqslant \pi, \tag{2.3}$$

$$|x_\alpha\rangle = \int_{-\pi}^{\pi} \frac{dk}{2\pi} e^{-ikx_\alpha}|k,\alpha\rangle \quad \text{for } x_\alpha = 0,1,2,\cdots, \tag{2.4}$$

we can transform the Hamiltonians H_α and $H_{\mathrm{d},\alpha}$ to

$$H_\alpha = \int_{-\pi}^{\pi} \frac{dk}{2\pi} E_k |k,\alpha\rangle\langle k,\alpha|, \tag{2.5}$$

$$H_{\mathrm{d},\alpha} = -t_\alpha \int_{-\pi}^{\pi} \frac{dk}{2\pi} \left(|k,\alpha\rangle\langle d_0| + \mathrm{h.c.}\right), \tag{2.6}$$

where the dispersion relation of the tight-binding model of a one-dimensional lead is

$$E_k = -2t\cos k \tag{2.7}$$

in the Brillouin zone $-\pi < k \leqslant \pi$.

The system (2.1) has bound states, scattering states, resonant states and anti-resonant states. Let us first present the bound states

$$\begin{cases} H|\psi_j\rangle &= E_j|\psi_j\rangle, \\ \langle\psi_j|H &= E_j\langle\psi_j|, \end{cases} \tag{2.8}$$

where the eigenvalues are $E_j = -2t\cos k_j \in \mathbb{R}$ and their eigen-wave-numbers k_j are pure imaginary with $\Im k_j > 0$. The bound eigenfunctions $|\psi_j\rangle$ have the orthonormal relation as follows

$$\langle\psi_i|\psi_j\rangle = \langle\psi_j|\psi_i\rangle = \delta_{ij}. \tag{2.9}$$

Due to some symmetries, some bound states may have $\langle d_0|\psi_j\rangle = 0$. Since such states do not affect conduction, we neglect them hereafter and assume that the number of contributing states is N. The bound states exponentially

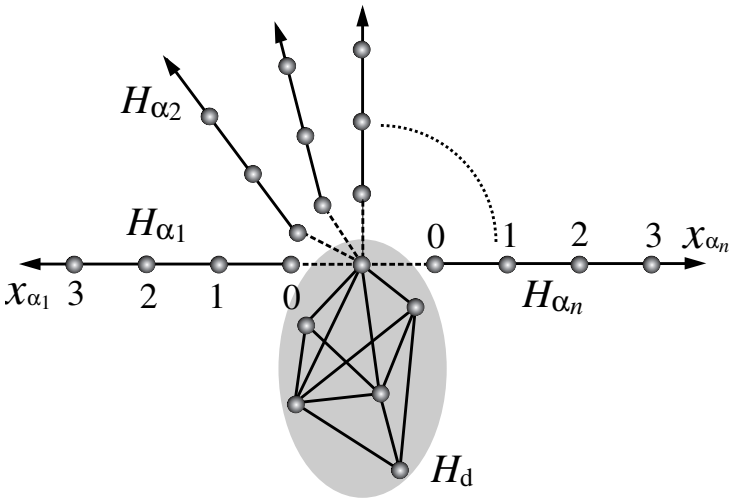

Figure 2.1: The open quantum N-level dot with the multiple leads that we consider in the present chapter.

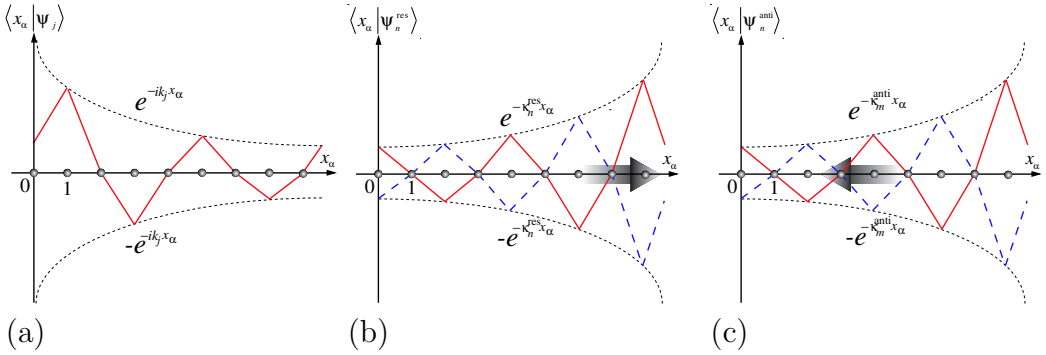

Figure 2.2: The eigenfunction of the bound states (a), resonant states (b) and anti-resonant states (c) in the lead α. Each solid line indicates the real part of the eigenfunction and each broken line indicates the imaginary part.

decay in the leads away from the central dot. They are not traveling wave, as shown in Fig. 2.2 (a);

$$|\langle x_\alpha|\psi_j\rangle| \propto e^{-(\Im k_j)x_\alpha}. \tag{2.10}$$

Let us second present the scattering states of the open quantum dot. Using the Lippmann-Schwinger equation as discussed in Appendix A, we obtain scattering states as

$$\begin{cases} |\psi_k^{\rm F}\rangle & = \sum_\alpha |\psi_{k,\alpha}^{\rm F}\rangle, \\ \langle\psi_k^{\rm F}| & \equiv |\psi_k^{\rm F}\rangle^\dagger \end{cases} \tag{2.11}$$

with the scattering state in the lead α

$$\begin{aligned} |\psi_{k,\alpha}^{\rm F}\rangle \equiv & \frac{1}{\sqrt{\langle\psi_{k,\alpha}^{\rm F}|\psi_{k,\alpha}^{\rm F}\rangle}} \left\{ |k,\alpha\rangle - t_\alpha \left(\sum_{j=0}^{N-1} |d_j\rangle\langle d_j|G^{\rm R}(E_k)|d_0\rangle \right.\right. \\ & \left.\left. -\langle d_0|G^{\rm R}(E_k)|d_0\rangle \sum_\beta \int_{-\pi}^{\pi} \frac{dq}{2\pi} \frac{t_\beta|q,\beta\rangle}{E_k - E_q + i\delta} \right) \right\} \\ = & \frac{1}{\sqrt{\langle\psi_{k,\alpha}^{\rm F}|\psi_{k,\alpha}^{\rm F}\rangle}} \left(|k,\alpha\rangle - t_\alpha|\psi_k^{\rm out}\rangle\right), \end{aligned} \tag{2.12}$$

where $|\psi_k^{\rm out}\rangle$ is the term of the outgoing wave, and we defined the retarded and advanced Green's functions as

$$G^{\rm R}(E) \equiv \frac{1}{E - H + i\delta}, \tag{2.13}$$

$$G^{\rm A}(E) = \left\{G^{\rm R}(E)\right\}^\dagger, \tag{2.14}$$

where δ is a positive infinitesimal. Each scattering state has its eigenvalue $E_k = -2t\cos k$ and is orthonormal to the each other,

$$H|\psi_k^{\rm F}\rangle = E_k|\psi_k^{\rm F}\rangle \ \text{ and } \ \langle\psi_k^{\rm F}|H = E_k\langle\psi_k^{\rm F}| \tag{2.15}$$

$$\langle\psi_k^{\rm F}|\psi_{k'}^{\rm F}\rangle = \delta(k - k'), \tag{2.16}$$

as well as is orthonormal to the bound eigenstates

$$\langle\psi_j|\psi_k^{\rm F}\rangle = \langle\psi_k^{\rm F}|\psi_j\rangle = 0. \tag{2.17}$$

Equation (2.15) can be proved as follows;

$$
\begin{aligned}
&H|\psi_k^{\rm F}\rangle = H\sum_\alpha |\psi_{k,\alpha}^{\rm F}\rangle = E_k \sum_\alpha |k,\alpha\rangle \\
&-\sum_\alpha t_\alpha \left\{ |d_0\rangle + \sum_{l=0}^{N-1} \langle d_l|G^{\rm R}(E_k)|d_0\rangle \left(\epsilon_l |d_l\rangle - \sum_{j=l+1}^{N-1} v_{lj}|d_j\rangle - \sum_{j=0}^{l-1} v_{jl}^*|d_j\rangle \right) \right. \\
&\left. -\langle d_0|G^{\rm R}(E_k)|d_0\rangle \sum_\beta \int_{-\pi}^{\pi} \frac{dq}{2\pi} \left(t_\beta |q,\beta\rangle + \frac{t_\beta E_q |q,\beta\rangle}{E_k - E_q + i\delta} - \frac{t_\beta^2}{E_k - E_q + i\delta}|d_0\rangle \right) \right\} \\
=&E_k \sum_\alpha |\psi_{k,\alpha}^{\rm F}\rangle \\
&+\sum_\alpha t_\alpha \left\{ \sum_{l=0}^{N-1} \langle d_l|G^{\rm R}(E_k)|d_0\rangle \left((E_k - \epsilon_l)\,|d_l\rangle + \sum_{j=l+1}^{N-1} v_{lj}|d_j\rangle + \sum_{j=0}^{l-1} v_{jl}^*|d_j\rangle \right) \right. \\
&\left. - \left(1 + \langle d_0|G^{\rm R}(E_k)|d_0\rangle \sum_\beta \int_{-\pi}^{\pi} \frac{dq}{2\pi} \frac{t_\beta^2}{E_k - E_q + i\delta} \right) |d_0\rangle \right\} \\
=&E_k|\psi_k^{\rm F}\rangle + \sum_\alpha t_\alpha \left\{ \left(\sum_{i=0}^{N-1} \langle d_0|(E_k - H + i\delta)|d_i\rangle \langle d_i|G^{\rm R}(E_k)|d_0\rangle - 1 \right) |d_0\rangle \right. \\
&\left. + \sum_{l=1}^{N-1} \left(\sum_{i=0}^{N-1} \langle d_l|E_k - H + i\delta|d_i\rangle \langle d_i|G^{\rm R}(E_k)|d_0\rangle \right) |d_l\rangle \right\} \\
=&E_k|\psi_k^{\rm F}\rangle + \sum_\alpha t_\alpha \left\{ \left(\langle d_0|d_0\rangle - 1 \right) |d_0\rangle + \sum_{l=1}^{N-1} \langle d_l|d_0\rangle |d_l\rangle \right\} \\
=&E_k|\psi_k^{\rm F}\rangle. \qquad (2.18)
\end{aligned}
$$

Equation (2.16) is proved as follows;

$$
\langle \psi_{k'}^{\rm F}|H|\psi_k^{\rm F}\rangle = \left\{ \begin{array}{ll} \langle \psi_{k'}^{\rm F}| \left(H|\psi_k^{\rm F}\rangle \right) & = E_k \langle \psi_{k'}^{\rm F}|\psi_k^{\rm F}\rangle \\ \left(\langle \psi_{k'}^{\rm F}|H \right) |\psi_k^{\rm F}\rangle & = E_{k'} \langle \psi_{k'}^{\rm F}|\psi_k^{\rm F}\rangle \end{array} \right. \qquad (2.19)
$$

and hence

$$
(E_k - E_{k'})\,\langle \psi_{k'}^{\rm F}|\psi_k^{\rm F}\rangle = 0. \qquad (2.20)
$$

R. G. Newton generally proved that the bound states and the scattering

states constitute the completeness of an open system [10];

$$\mathbf{1} = \sum_j |\psi_j\rangle\langle\psi_j| + \int_{-\pi}^{\pi} \frac{dk}{2\pi} |\psi_k^{\mathrm{F}}\rangle\langle\psi_k^{\mathrm{F}}|. \tag{2.21}$$

2.2 Resonant states of the open quantum dot

In the present section, we generally define resonant states of an open quantum dot [11]. We seek discrete and generally complex eigenvalues E_l^{res} of the resonant states of the whole system;

$$H|\psi_l^{\mathrm{res}}\rangle = E_l^{\mathrm{res}}|\psi_l^{\mathrm{res}}\rangle, \tag{2.22}$$

$$\langle\tilde{\psi}_l^{\mathrm{res}}|H = E_l^{\mathrm{res}}\langle\tilde{\psi}_l^{\mathrm{res}}|, \tag{2.23}$$

where $|\psi_l^{\mathrm{res}}\rangle$ is the right-eigenfunction and $\langle\tilde{\psi}_l^{\mathrm{res}}|$ is the left-eigenfunction. The resonant eigenfunctions satisfies the boundary condition of an outgoing and diverging wave as [11]

$$\langle x_\alpha|\psi_l^{\mathrm{res}}\rangle \propto e^{ik_l^{\mathrm{res}}x_\alpha}, \tag{2.24}$$

$$\langle\tilde{\psi}_l^{\mathrm{res}}|x_\alpha\rangle \propto e^{ik_l^{\mathrm{res}}x_\alpha} \tag{2.25}$$

for x_α on any lead α. Note that the resonant eigen-wave-number $k_l^{\mathrm{res}} \equiv k_{\mathrm{r}l}^{\mathrm{res}} + i\kappa_l^{\mathrm{res}}$ is generally a complex number with its real part $k_{\mathrm{r}l}^{\mathrm{res}} > 0$ and its imaginary part $\kappa_l^{\mathrm{res}} < 0$ [11]; the resonant state

$$\langle x_\alpha|\psi_l^{\mathrm{res}}\rangle \propto e^{ik_{\mathrm{r}l}^{\mathrm{res}}x_\alpha} e^{-\kappa_l^{\mathrm{res}}x_\alpha} \tag{2.26}$$

hence describes a wave flowing in the positive x_α direction and diverging exponentially as shown in Fig. 2.2 (b). The resonant eigenvalue E_l^{res} is given by the dispersion relation (2.7) with the eigen-wave-number k_l^{res}. It is hence also generally complex as follows;

$$\begin{aligned} E_l^{\mathrm{res}} &\equiv E_{\mathrm{r}l}^{\mathrm{res}} + iE_{\mathrm{i}l}^{\mathrm{res}} = -2t\cos k_l^{\mathrm{res}} \\ &= -2t\cos k_{\mathrm{r}l}^{\mathrm{res}}\cosh\kappa_l^{\mathrm{res}} + 2ti\sin k_{\mathrm{r}l}^{\mathrm{res}}\sinh\kappa_l^{\mathrm{res}}, \end{aligned} \tag{2.27}$$

where $E_{\mathrm{r}l}^{\mathrm{res}}$ is the real part of the eigenvalue and $E_{\mathrm{i}l}^{\mathrm{res}}$ (< 0) is the imaginary part. The entire eigenfunction of the resonant state can be given by

substituting a resonant eigen-wave-number $k_l^{\rm res}$ for the wave number k of the outgoing wave term $|\psi_k^{\rm out}\rangle$ of the scattering state (2.12);

$$
\begin{aligned}
&|\psi_l^{\rm res}\rangle \equiv |\psi_k^{\rm out}\rangle\big|_{k=k_l^{\rm res}} \\
=&N_l^{\rm res}\left(\sum_{i=0}|d_i\rangle\langle d_i|G^{\rm R}(E_l^{\rm res})|d_0\rangle + \langle d_0|G^{\rm R}(E_l^{\rm res})|d_0\rangle\sum_\alpha\frac{t_\alpha}{t}\sum_{x_\alpha=0}^{\infty}e^{ik_l^{\rm res}x_\alpha}|x_\alpha\rangle\right),
\end{aligned}
\tag{2.28}
$$

except that the normalization coefficient $N_l^{\rm res}$ is not fixed yet.

The resonant eigenfunctions are bi-orthonormal to each other;

$$\langle\tilde{\psi}_{l'}^{\rm res}|\psi_l^{\rm res}\rangle^{(g)} = \delta_{ll'}. \tag{2.29}$$

We stress that the inner product $\langle\cdot|\cdot\rangle^{(g)}$ of Eq. (2.29) is different from the inner product in the Hilbert space. In the next subsection, we argue in detail a definition of the inner product in the extended Hilbert space.

We also define anti-resonant states of the system;

$$H|\psi_m^{\rm anti}\rangle = E_m^{\rm anti}|\psi_m^{\rm anti}\rangle, \tag{2.30}$$

$$\langle\tilde{\psi}_m^{\rm anti}|H = E_m^{\rm anti}\langle\tilde{\psi}_m^{\rm anti}| \tag{2.31}$$

with the anti-resonant eigenvalues $E_m^{\rm anti} \equiv (E_l^{\rm res})^*$, its right-eigenfunction $|\psi_m^{\rm anti}\rangle \equiv |\tilde{\psi}_l^{\rm res}\rangle$ and its left-eigenfunction $\langle\tilde{\psi}_m^{\rm anti}| \equiv \langle\psi_l^{\rm res}|$. The anti-resonant state has the complex wave-number $k_m^{\rm anti} = -(k_l^{\rm res})^*$, and satisfies the boundary condition of an incoming and diverging wave as

$$\langle x_\alpha|\psi_m^{\rm anti}\rangle = e^{ik_m^{\rm anti}x_\alpha}, \tag{2.32}$$

$$\langle\tilde{\psi}_m^{\rm anti}|x_\alpha\rangle = e^{ik_m^{\rm anti}x_\alpha}. \tag{2.33}$$

Note that anti-resonant eigen-wave-number $k_m^{\rm anti} \equiv {k_{\rm r}}_m^{\rm anti} + i\kappa_m^{\rm anti}$ satisfies ${k_{\rm r}}_m^{\rm anti}, \kappa_m^{\rm anti} < 0$; the anti-resonant state

$$\langle x_\alpha|\psi_m^{\rm anti}\rangle \propto e^{i{k_{\rm r}}_m^{\rm anti}x_\alpha}e^{-\kappa_m^{\rm anti}x_\alpha} = e^{-i{k_{\rm r}}_l^{\rm res}x_\alpha}e^{-\kappa_l^{\rm res}x_\alpha} \tag{2.34}$$

hence describes time reversal of the resonant state as shown in Fig. 2.2 (c). The anti-resonant eigenvalue $E_m^{\rm anti}$ is given by

$$
\begin{aligned}
E_m^{\rm anti} &\equiv {E_{\rm r}}_m^{\rm anti} + i{E_{\rm i}}_m^{\rm anti} = -2t\cos k_m^{\rm anti} \\
&= -2t\cos {k_{\rm r}}_m^{\rm anti}\cosh\kappa_l^{\rm anti} + 2ti\sin {k_{\rm r}}_m^{\rm anti}\sinh\kappa_m^{\rm anti} \\
&= -2t\cos {k_{\rm r}}_m^{\rm res}\cosh\kappa_m^{\rm res} - 2ti\sin {k_{\rm r}}_m^{\rm res}\sinh\kappa_m^{\rm res} \\
&= {E_{\rm r}}_m^{\rm res} - i{E_{\rm i}}_m^{\rm res} = (E_m^{\rm res})^*,
\end{aligned}
\tag{2.35}
$$

with its imaginary part $E_{\mathrm{i}m}^{\mathrm{anti}} > 0$. Similarly to Eq. (2.28), the entire eigenfunction of the anti-resonant state can be given by

$$\begin{aligned}
&|\psi_m^{\mathrm{anti}}\rangle \equiv |\psi_k^{\mathrm{in}}\rangle\big|_{k=k_m^{\mathrm{anti}}} = |\psi_k^{\mathrm{out}}\rangle^*\big|_{k=k_m^{\mathrm{anti}}} \\
=&N_m^{\mathrm{anti}} \left(\sum_{i=0}^{N-1} |d_i\rangle\langle d_i|G^{\mathrm{A}}(E_m^{\mathrm{anti}})|d_0\rangle + \langle d_0|G^{\mathrm{A}}(E_m^{\mathrm{anti}})|d_0\rangle \sum_\alpha \frac{t_\alpha}{t} \sum_{x_\alpha=0}^{\infty} e^{ik_m^{\mathrm{anti}} x_\alpha} |x_\alpha\rangle \right).
\end{aligned} \tag{2.36}$$

The anti-resonant states also have the bi-orthonormal relation

$$\langle \tilde{\psi}_{m'}^{\mathrm{anti}} | \psi_m^{\mathrm{anti}} \rangle^{(g)} \equiv \delta_{mm'}. \tag{2.37}$$

Here we summarize the eigen-wave-numbers and eigenvalues of the bound, resonant and anti-resonant states in Fig. 2.3. The eigen-wave-number k_j of a bound state is either on the imaginary k axis or on the line $\Re k = \pi$. (In systems with continuous space, the bound states exist only on the imaginary k axis; the bound states on the line $\Re k = \pi$ appear because the leads of the present system are lattice systems.) The eigen-wave-number k_l^{res} of a resonant state is on the fourth quadrant of the complex wave-number plane. The eigen-wave-number k_m^{anti} of an anti-resonant state is on the third quadrant of the complex wave-number plane.

Upon mapping the complex wave-number plane to the complex energy plane through the dispersion relation $E = -2t\cos k$, we have two Riemann sheets. The bound eigenvalues are located on the real axis of the first Riemann sheet of the complex energy plane with $|E_j| > 2t$. The resonant eigenvalues are on the lower half plane of the second Riemann sheet, while the anti-resonant eigenvalues are on the upper half plane of the same sheet. There are a branch cut $|E| < 2t$ and two branch points $E = \pm 2t$ connecting the two Riemann sheets.

2.2.1 Definition of the inner product in the extended Hilbert space

In the present subsection, we give a definition of the inner product of resonant eigenfunctions [12]. The resonant states generally have diverging and outgoing wave functions away from the central dot, so that the inner product $\langle \tilde{\psi}_l^{\mathrm{res}} | \psi_l^{\mathrm{res}} \rangle$ would also diverge if we used the standard definition in the

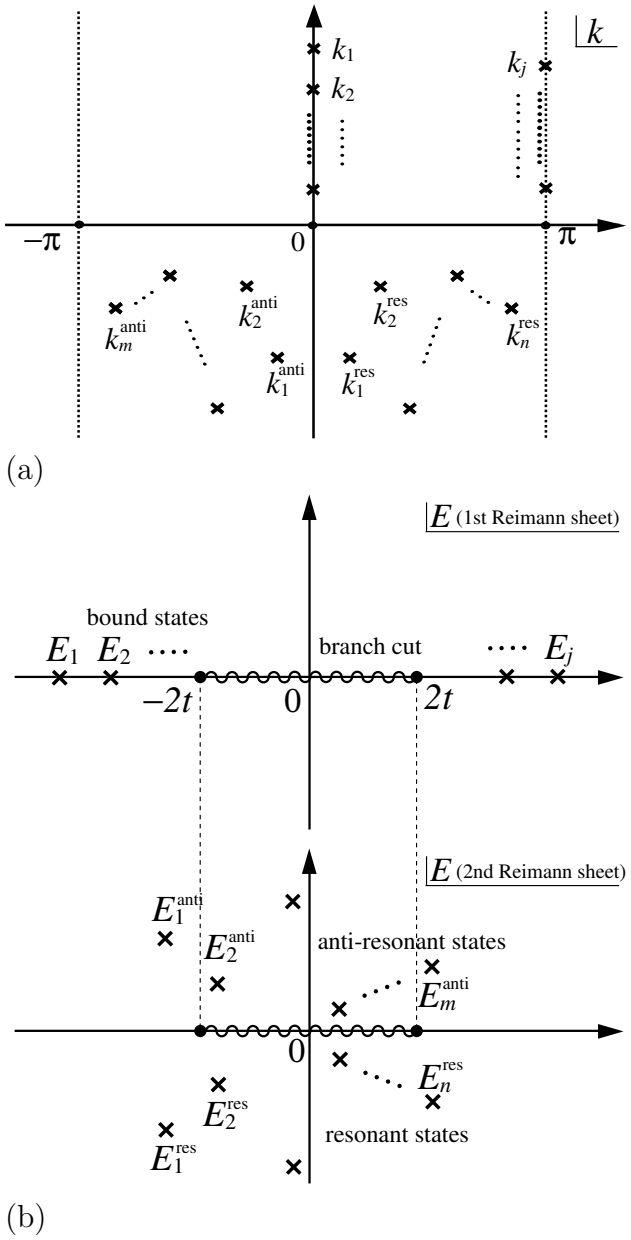

Figure 2.3: (a) Distribution of the bound eigen-wave-numbers k_j, resonant eigen-wave-numbers $k_l^{\rm res}$ and anti-resonant eigen-wave-numbers $k_l^{\rm res}$ on the complex wave-number plane. (b) Distribution of the bound eigenvalues E_j, resonant eigenvalues $E_l^{\rm res}$ and anti-resonant eigenvalues $E_m^{\rm anti}$ on the complex energy plane.

Hilbert space. To avoid this problem a definition of the inner product in the extended Hilbert space has been introduced;

$$\langle\tilde{\psi}_l^{\rm res}|\psi_l^{\rm res}\rangle^{(g)} \equiv \lim_{g\to+0}\left(\sum_\alpha\sum_{x_\alpha=0}^{\infty}\langle\tilde{\psi}_l^{\rm res}|x_\alpha^{(g)}\rangle\langle x_\alpha^{(g)}|\psi_l^{\rm res}\rangle\right) + \sum_{i=0}^{N-1}\langle\tilde{\psi}_l^{\rm res}|d_i\rangle\langle d_i|\psi_l^{\rm res}\rangle, \tag{2.38}$$

with

$$|x_\alpha^{(g)}\rangle \equiv e^{-gx_\alpha}|x_\alpha\rangle. \tag{2.39}$$

The convergent factor g must take a positive and sufficiently large value when we calculate the summation over x_α. It is introduced to suppress the divergence indicated in Eqs. (2.26) and (2.34). Note that the inner product of the bound states in the extended Hilbert space coincides with the inner product in the Hilbert space.

The definition (2.38) is equivalent to modify an integration contour in the complex wave-number plane in the following way (Fig. 2.4). Instead of the integration contour in Fig. 2.4 (a), we first consider an integration contour in Fig. 2.4 (b) with a large and negative imaginary part. The contour must be low enough so that all resonant states may be above it. We then move the integration contour upward until it comes upon the real axis of the complex wave-number plane. On its way upward, the contour must enclose all resonant states as in Fig. 2.4 (c). In other words, we carry out the following procedure;

$$\begin{aligned}
&\sum_{x_\alpha=0}^{\infty}\langle\tilde{\psi}_l^{\rm res}|x_\alpha^{(g)}\rangle\langle x_\alpha^{(g)}|\psi_l^{\rm res}\rangle = \sum_{x_\alpha=0}^{\infty} e^{-gx_\alpha}\langle\tilde{\psi}_l^{\rm res}|x_\alpha\rangle\langle x_\alpha|\psi_l^{\rm res}\rangle e^{-gx_\alpha} \\
&= \int_{-\pi}^{\pi}\frac{dk}{2\pi}\int_{-\pi}^{\pi}\frac{dk'}{2\pi}\langle\tilde{\psi}_l^{\rm res}|k+ig,\alpha\rangle\langle k'+ig,\alpha|\psi_l^{\rm res}\rangle\sum_{x_\alpha=0}^{\infty}e^{i(k'-k)x_\alpha} \\
&= \int_{-\pi}^{\pi}\frac{dk}{2\pi}\langle\tilde{\psi}_l^{\rm res}|k+ig,\alpha\rangle\langle k+ig,\alpha|\psi_l^{\rm res}\rangle \\
&= \int_{-\pi-ig}^{\pi-ig}\frac{dk}{2\pi}\langle\tilde{\psi}_l^{\rm res}|k,\alpha\rangle\langle k,\alpha|\psi_l^{\rm res}\rangle.
\end{aligned} \tag{2.40}$$

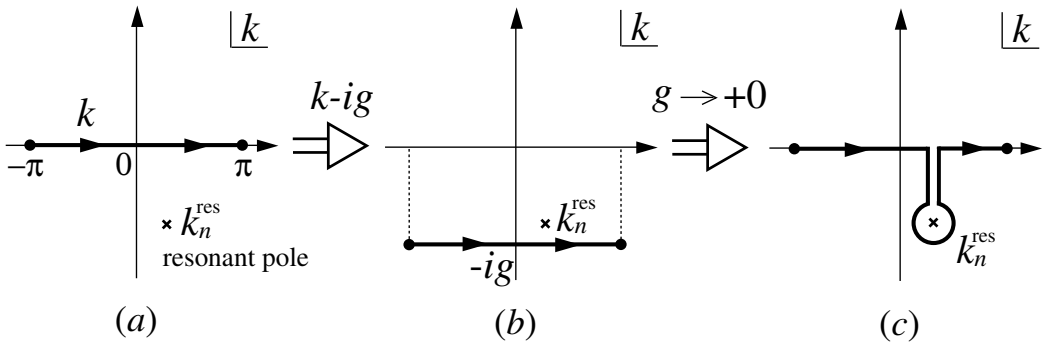

Figure 2.4: A definition of the inner product of the resonant states in the complex wave-number plane.

Hence Eq. (2.38) can be rewritten in the form

$$\langle\tilde{\psi}_l^{\rm res}|\psi_l^{\rm res}\rangle^{(g)} = \lim_{g\to+0}\sum_{\alpha}\int_{-\pi-ig}^{\pi-ig}\frac{dk}{2\pi}\langle\tilde{\psi}_l^{\rm res}|k,\alpha\rangle\langle k,\alpha|\psi_l^{\rm res}\rangle + \sum_{i=0}^{N-1}\langle\tilde{\psi}_l^{\rm res}|d_i\rangle\langle d_i|\psi_l^{\rm res}\rangle. \tag{2.41}$$

2.2.2 A normalization coefficient of resonant states

We next fix the normalization coefficient $N_l^{\rm res}(\in\mathbb{C})$ of the resonant state (2.28), using the inner product (2.38). We have the inner product as

$$\begin{aligned}\langle\tilde{\psi}_l^{\rm res}|\psi_l^{\rm res}\rangle^{(g)} &= (N_l^{\rm res})^2\left\{\sum_{i=0}^{N-1}\langle d_0|G^{\rm R}(E_l^{\rm res})|d_i\rangle\langle d_i|G^{\rm R}(E_l^{\rm res})|d_0\rangle\right.\\ &\qquad\left.+\left(\langle d_0|G^{\rm R}(E_l^{\rm res})|d_0\rangle\right)^2\lim_{g\to+0}\sum_{\alpha}\left(\frac{t_\alpha}{t}\right)^2\sum_{x_\alpha=0}^{\infty}e^{2\left(-g+ik_l^{\rm res}\right)x_\alpha}\right\},\end{aligned} \tag{2.42}$$

$$= (N_l^{\rm res})^2\left\{\frac{\bar{t}^2\left(\langle d_0|G^{\rm R}(E_l^{\rm res})|d_0\rangle\right)^2}{1-e^{2ik_l^{\rm res}}}+\sum_{i=0}^{N-1}\langle d_0|G^{\rm R}(E_l^{\rm res})|d_i\rangle\langle d_i|G^{\rm R}(E_l^{\rm res})|d_0\rangle\right\}. \tag{2.43}$$

Thus we obtain the normalization coefficient of the resonant states as

$$N_l^{\rm res} = \left\{ \frac{\bar{t^2}\left(\langle d_0|G^{\rm R}(E_l^{\rm res})|d_0\rangle\right)^2}{1-e^{2ik_l^{\rm res}}} + \sum_{i=0}^{N-1}\langle d_0|G^{\rm R}(E_l^{\rm res})|d_i\rangle\langle d_i|G^{\rm R}(E_l^{\rm res})|d_0\rangle \right\}^{-\frac{1}{2}}, \tag{2.44}$$

By the same token, we obtain the normalization coefficient of the anti-resonant eigenfunction (2.36) as

$$\begin{aligned} N_m^{\rm anti} &= \left\{ \frac{\bar{t^2}\left(\langle d_0|G^{\rm A}(E_m^{\rm anti})|d_0\rangle\right)^2}{1-e^{2ik_m^{\rm anti}}} + \sum_{i=0}^{N-1}\langle d_0|G^{\rm A}(E_m^{\rm anti})|d_i\rangle\langle d_i|G^{\rm A}(E_m^{\rm anti})|d_0\rangle \right\}^{-\frac{1}{2}} \\ &= (N_m^{\rm res})^*. \end{aligned} \tag{2.45}$$

Here we summarize the bound states $|\psi_j\rangle$, resonant states $|\psi_l^{\rm res}\rangle$ and anti-resonant states $|\psi_m^{\rm anti}\rangle$ as the discrete eigenstates $|\psi_n\rangle$. We newly define the discrete eigenstates as

$$H|\psi_n\rangle = E_n|\psi_n\rangle \tag{2.46}$$

$$\langle\tilde{\psi}_n|H = \langle\tilde{\psi}_n|E_n \tag{2.47}$$

with $|\psi_n\rangle \in \left\{|\psi_j\rangle, |\psi_l^{\rm res}\rangle, |\psi_m^{\rm anti}\rangle\right\}$ and $\langle\tilde{\psi}_n| \in \left\{\langle\psi_j|, \langle\tilde{\psi}_l^{\rm res}|, \langle\tilde{\psi}_m^{\rm anti}|\right\}$. They all are bi-orthonormal to each other;

$$\langle\tilde{\psi}_n|\psi_{n'}\rangle^{(g)} = \delta_{nn'}. \tag{2.48}$$

The quantum number n runs from 1 to $2N$, where each number of the bound, resonant and anti-resonant states depends on the structure of the central dot.

2.2.3 Calculation of eigenstates for the discrete eigenstates

We now briefly describe a method of computing all discrete eigenvalues using a finite effective Hamiltonian $H_{\rm eff}(E)$ with a complex effective potential $V_{\rm eff}(E)$ [1]. The effective Hamiltonian is defined so that the Green's function of the whole system may be equal to that of the effective system for the sites on the central dot;

$$\langle d_i|G^{\rm R}(E)|d_j\rangle = \langle d_i|G^{\rm R}_{\rm eff}(E)|d_j\rangle \equiv \langle d_i|\frac{1}{E-H_{\rm eff}(E)+i\delta}|d_j\rangle \tag{2.49}$$

with

$$H_{\rm eff}(E) \equiv H_{\rm d} + \sum_{\alpha} V_{\rm eff}^{(\alpha)}(E)|d_0\rangle\langle d_0|. \tag{2.50}$$

The effective potential $V^{(\alpha)}(E)$ is equivalent to the self-energy of the semi-infinite lead α and represents an effect of the boundary condition of an outgoing wave [13]. In the present case, the effective potential is given in the form

$$V_{\rm eff}^{(\alpha)}(E) = -\frac{t_\alpha^2}{t} z_E = (\bar{t_\alpha})^2 \, \frac{E - i\sqrt{4t^2 - E^2}}{2}, \tag{2.51}$$

where $z_E \equiv e^{ik_E}$ $(\Re k_E \geqslant 0)$ and $\bar{t_\alpha} \equiv t_\alpha/t$ denotes the normalized hopping energy between the dot and the lead α. See Appendix B for an easy way of calculating the effective potential.

The effective Hamiltonian (2.50) is a non-Hermitian energy-dependent operator. The discrete eigenvalues $E = E_n$ of bound and resonant states are given as poles of the Green's function (2.49). Hence we solve the secular equation for the effective Hamiltonian;

$$\det\left(E_n - H_{\rm eff}(E_n)\right) = 0. \tag{2.52}$$

Since we used the retarded Green's function in (2.49), Eq. (2.52) does not produce anti-resonant states. The anti-resonant states are given by using the advanced Green's function in (2.49). Then we obtain the advanced effective Hamiltonian

$$H_{\rm eff}^{*}(E) = H_{\rm d} + \sum_{\alpha} V_{\rm eff}^{(\alpha)}(E)^{*}|d_0\rangle\langle d_0|. \tag{2.53}$$

The secular equation for the effective Hamiltonian (2.53),

$$\det\left(E_n - H_{\rm eff}^{*}(E_n)\right) = 0, \tag{2.54}$$

produces the anti-resonant states instead of the resonant states. Indeed, the left-hand side of Eq. (2.54) is equal to

$$\det\left(E_n - H_{\rm eff}^{*}(E_n)\right) = \det\left(E_n^{*} - H_{\rm eff}(E_n^{*})\right)^{*}, \tag{2.55}$$

which gives complex conjugate of the solutions of Eq. (2.52). Then we also obtain the eigen-wave-number k_n from the dispersion relation and the corresponding eigenfunction of Eqs. (2.28) and (2.36).

2.3 Relation of the Green's function and the discrete eigenstates

In the present section, we show the contribution of resonant states to the retarded Green's function. Using the completeness (2.21), we first express the Green's functions in the spectral representation;

$$G^{\mathrm{R}}(E) = \sum_j \frac{|\psi_j\rangle\langle\psi_j|}{E - E_j} + \int_{C^{\mathrm{R}}_{\mathrm{B.Z.}}} \frac{dk}{2\pi} \frac{|\psi^{\mathrm{F}}_k\rangle\langle\psi^{\mathrm{F}}_k|}{E - E_k}, \tag{2.56}$$

$$G^{\mathrm{A}}(E) = \sum_j \frac{|\psi_j\rangle\langle\psi_j|}{E - E_j} + \int_{C^{\mathrm{A}}_{\mathrm{B.Z.}}} \frac{dk}{2\pi} \frac{|\psi^{\mathrm{F}}_k\rangle\langle\psi^{\mathrm{F}}_k|}{E - E_k}, \tag{2.57}$$

where the integration contours $C^{\mathrm{R}}_{\mathrm{B.Z.}}$ and $C^{\mathrm{A}}_{\mathrm{B.Z.}}$ are indicated in Fig. 2.5.

Next, we displace the integration contours $C^{\mathrm{R}}_{\mathrm{B.Z.}}$ and $C^{\mathrm{A}}_{\mathrm{B.Z.}}$ as shown in Fig. 2.6. The residues integrals of the resonant states k^{res}_l and anti-resonant states k^{anti}_m are reduced to

$$\oint_{C(k=k^{\mathrm{res}}_l)} \frac{dk}{2\pi} \frac{|\psi^{\mathrm{F}}_k\rangle\langle\psi^{\mathrm{F}}_k|}{E - E_k} = \frac{|\psi^{\mathrm{res}}_l\rangle\langle\tilde{\psi}^{\mathrm{res}}_l|}{E - E^{\mathrm{res}}_l}, \tag{2.58}$$

$$\oint_{C(k=k^{\mathrm{anti}}_m)} \frac{dk}{2\pi} \frac{|\psi^{\mathrm{F}}_k\rangle\langle\psi^{\mathrm{F}}_k|}{E - E_k} = \frac{|\psi^{\mathrm{res}}_m\rangle\langle\tilde{\psi}^{\mathrm{anti}}_m|}{E - E^{\mathrm{anti}}_m}. \tag{2.59}$$

We then have

$$\begin{aligned} G^{\mathrm{R}}(E) =& \sum_j \frac{|\psi_j\rangle\langle\psi_j|}{E - E_j} + \sum_l \frac{|\psi^{\mathrm{res}}_l\rangle\langle\tilde{\psi}^{\mathrm{res}}_l|}{E - E^{\mathrm{res}}_l} \\ &+ \lim_{\kappa_0 \to +\infty} \int_{C^{\mathrm{R}}_{\perp}(\kappa_0) + C^{\mathrm{R}}_{\parallel}(\kappa_0)} \frac{dk}{2\pi} \frac{|\psi^{\mathrm{F}}_k\rangle\langle\psi^{\mathrm{F}}_k|}{E - E_k}, \end{aligned} \tag{2.60}$$

$$\begin{aligned} G^{\mathrm{A}}(E) =& \sum_j \frac{|\psi_j\rangle\langle\psi_j|}{E - E_j} + \sum_m \frac{|\psi^{\mathrm{anti}}_m\rangle\langle\tilde{\psi}^{\mathrm{anti}}_m|}{E - E^{\mathrm{anti}}_m} \\ &+ \lim_{\kappa_0 \to +\infty} \int_{C^{\mathrm{A}}_{\perp}(\kappa_0) + C^{\mathrm{A}}_{\parallel}(\kappa_0)} \frac{dk}{2\pi} \frac{|\psi^{\mathrm{F}}_k\rangle\langle\psi^{\mathrm{F}}_k|}{E - E_k}. \end{aligned} \tag{2.61}$$

We thus extract the resonant and anti-resonant states. Note that κ_0 of the modified integration contour must be positive and larger than the imaginary

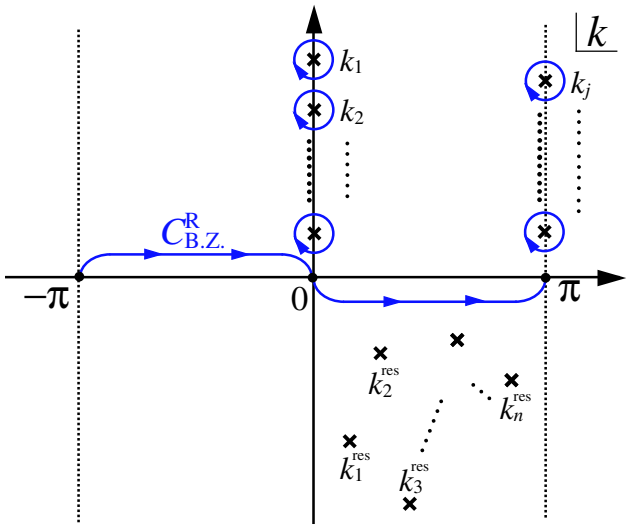

(a)

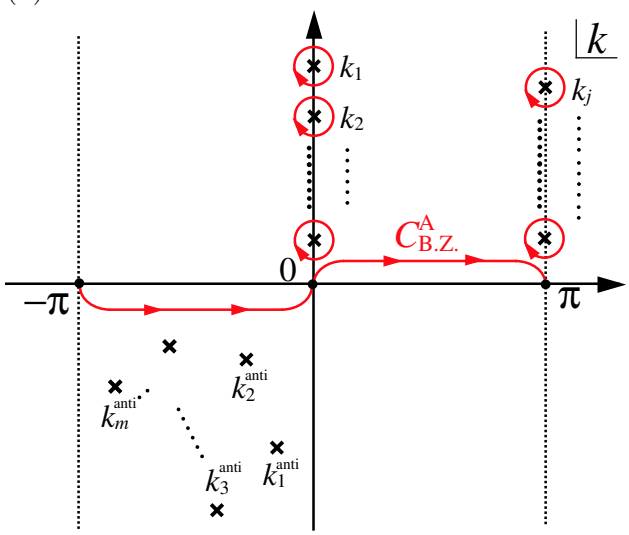

(b)

Figure 2.5: (a) An integration contour for the retarded Green's function and (b) for the advanced Green's function, with the circular contours extracting bound states in the complex wave-number plane.

parts of all the resonant eigen-wave-numbers. On the other hand, we numerically found that the contributions of the parallel integration contours $C_{\parallel}^{\rm R}(\kappa_0)$ and $C_{\parallel}^{\rm A}(\kappa_0)$ vanish for the states on the central dot;

$$\lim_{\kappa_0\to+\infty}\int_{C_{\parallel}^{\rm R}(\kappa_0)}\frac{dk}{2\pi}\frac{|\psi_k^{\rm F}\rangle\langle\psi_k^{\rm F}|}{E-E_k}+\int_{C_{\parallel}^{\rm A}(\kappa_0)}\frac{dk}{2\pi}\frac{|\psi_k^{\rm F}\rangle\langle\psi_k^{\rm F}|}{E-E_k}=0. \tag{2.62}$$

The relation can be analytically proved for $N = 2$. On the other hand, Eq. (2.62) does not seen to hold if the semi-infinite leads are not attached to a single site of the central dot. This is why we are focused on the present system (2.1).

Finally, we add the retarded and advanced Green's functions;

$$\begin{aligned}G^{\rm R}(E)+G^{\rm A}(E)=&2\sum_j\frac{|\psi_j\rangle\langle\psi_j|}{E-E_j}+\sum_l\frac{|\psi_l^{\rm res}\rangle\langle\psi_l^{\rm res}|}{E-E_l^{\rm res}}+\sum_m\frac{|\psi_m^{\rm anti}\rangle\langle\psi_m^{\rm anti}|}{E-E_m^{\rm anti}}\\&+\int_{C_\perp^{\rm R}+C_\perp^{\rm A}}\frac{dk}{2\pi}\frac{|\psi_k^{\rm F}\rangle\langle\psi_k^{\rm F}|}{E-E_k}.\end{aligned} \tag{2.63}$$

The sum of the contributions of the integration contour $C_\perp^{\rm R}$ and $C_\perp^{\rm A}$ is equal to the contribution of the bound states except for the sign;

$$\int_{C_\perp^{\rm R}+C_\perp^{\rm A}}\frac{dk}{2\pi}\frac{|\psi_k^{\rm F}\rangle\langle\psi_k^{\rm F}|}{E-E_k}=\sum_j\oint_{C(k=k_j)}\frac{dk}{2\pi}\frac{|\psi_k^{\rm F}\rangle\langle\psi_k^{\rm F}|}{E-E_k}=-\sum_j\frac{|\psi_j\rangle\langle\psi_j|}{E-E_j}. \tag{2.64}$$

Thus we find that the sum of the retarded and advanced Green's functions is equal to the contributions of only the discrete eigenstates for the states on the central dot;

$$G^{\rm A}(E)+G^{\rm R}(E)=\Lambda(E), \tag{2.65}$$

where

$$\Lambda(E)\equiv\sum_{n\in j,l,m}\frac{|\psi_n\rangle\langle\tilde{\psi}_n|}{E-E_n}. \tag{2.66}$$

It is noteworthy here that the difference between the retarded and advanced Green's function is known to be given by [1]

$$G^{\rm A}(E)-G^{\rm R}(E)=iG^{\rm R}(E)\Gamma(E)G^{\rm A}(E), \tag{2.67}$$

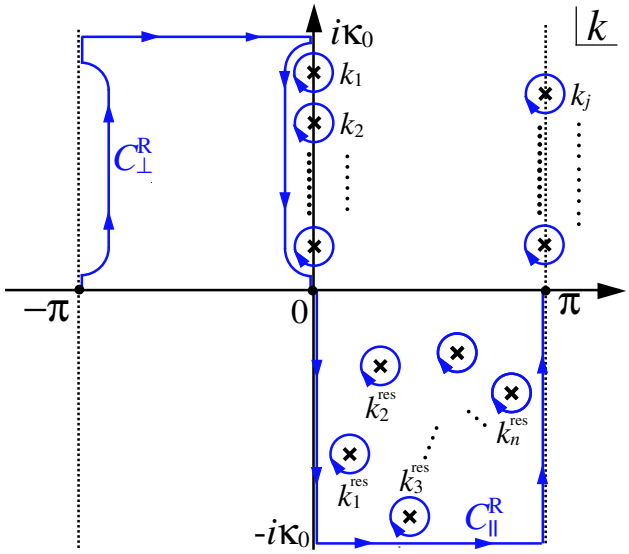

(a)

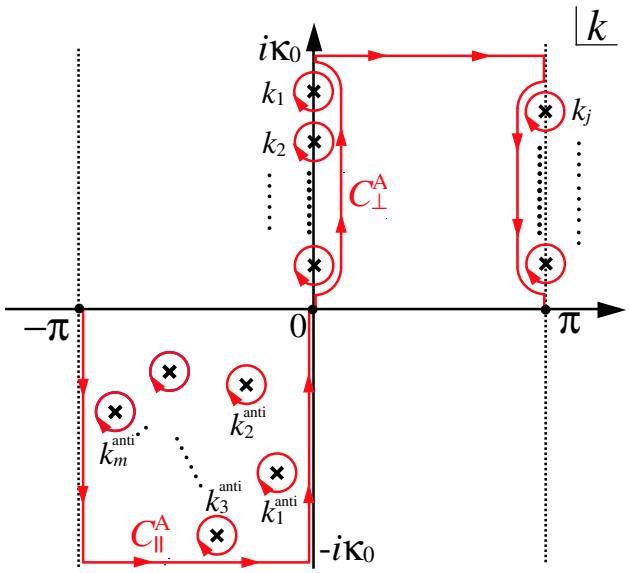

(b)

Figure 2.6: (a) An integration contour of the retarded Green's function, modified for extracting the resonant states in the complex wave-number plane. (b) An integration contour of the advanced Green's function, modified for extracting the anti-resonant states.

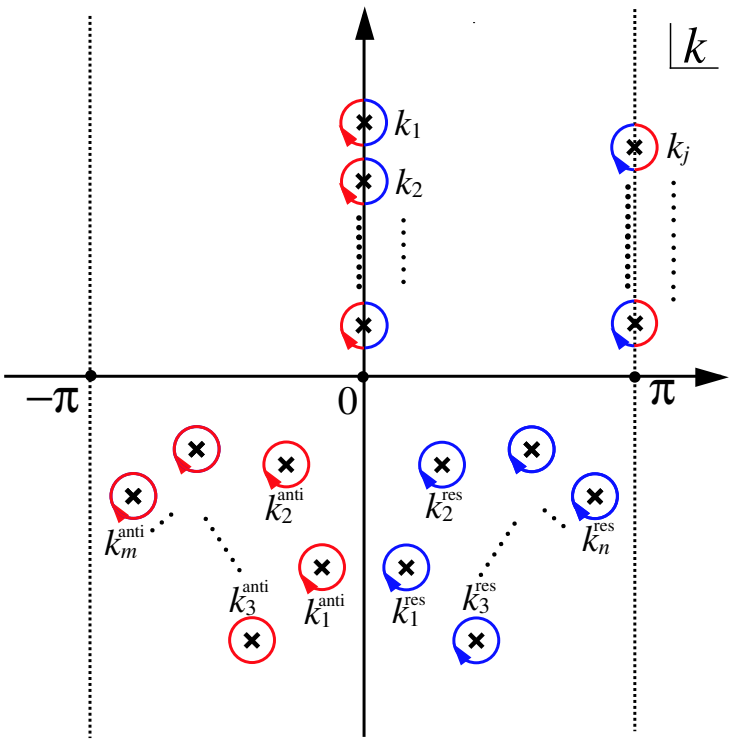

Figure 2.7: The sum of the modified integration contour of the retarded and advanced Green's functions in the complex wave-number plane.

where

$$\Gamma(E) \equiv \sum_{\alpha} \Gamma^{(\alpha)}(E), \tag{2.68}$$

$$\begin{aligned}\Gamma^{(\alpha)}(E) &\equiv i\left[V_{\text{eff}}^{(\alpha)}(E) - \left(V_{\text{eff}}^{(\alpha)}(E)\right)^{*}\right]|d_0\rangle\langle d_0| \\ &= (\bar{t_\alpha})^2\sqrt{4t^2 - E^2}|d_0\rangle\langle d_0|.\end{aligned} \tag{2.69}$$

Equation (2.65) shows that the real part of the Green's function is given by the discrete eigenstates, while Eq. (2.67) shows that the imaginary part of the Green's function is given by the inverse of branch point singularity [1]. Using the simultaneous matrix equation of Eqs. (2.65) and (2.67), we can construct the Green's function with the discrete eigenstates and the branch point singularity.

2.4 Conductance consisted of the discrete eigenstates and the branch points

In the present section, we derive a simple conductance formula showing that the conductance of the system (2.1) consists of the contributions from the discrete states and the branch points. Equations (2.65) and (2.67) give the matrix Riccati equation

$$G^{\text{R/A}}(E)\left(\pm i\Gamma(E)\right)G^{\text{R/A}}(E) - \left\{2 + \Lambda(E)\left(\pm i\Gamma(E)\right)\right\}G^{\text{R/A}}(E) + \Lambda(E) = 0, \tag{2.70}$$

which gives the elements of the Green's functions as follows:

$$\begin{aligned}\langle d_i|G^{\text{R}}(E)|d_j\rangle =& \frac{\langle d_i|\Lambda(E)|d_j\rangle}{2} - i\frac{\langle d_i|\Lambda(E)|d_0\rangle\langle d_0|\Lambda(E)|d_j\rangle}{\langle d_0|\Lambda(E)|d_0\rangle^2} \\ &\times\left\{\frac{1}{\langle d_0|\Gamma(E)|d_0\rangle} \pm \sqrt{\left(\frac{1}{\langle d_0|\Gamma(E)|d_0\rangle}\right)^2 - \left(\frac{\langle d_0|\Lambda(E)|d_0\rangle}{2}\right)^2}\right\},\end{aligned} \tag{2.71}$$

where the sign $\pm$ is dependent on the structure of the central dot. Using the Fisher-Lee relation [14], we can obtain the conductance $\mathcal{G}_{\alpha\to\beta}(E)$ from the

lead α to the lead β;

$$\begin{aligned}\mathcal{G}_{\alpha\to\beta}(E) &\equiv \frac{2e^2}{h}\mathrm{Tr}\left\{\Gamma^{(\beta)}(E)G^{\mathrm{R}}(E)\Gamma^{(\alpha)}(E)G^{\mathrm{A}}(E)\right\} \\ &= \langle d_0|\Gamma^{(\beta)}(E)|d_0\rangle\langle d_0|\Gamma^{(\alpha)}(E)|d_0\rangle\left|\langle d_0|G^{\mathrm{R}}(E)|d_0\rangle\right|^2 \\ &= \frac{4e^2}{h}\left(\frac{\bar{t}_\alpha\bar{t}_\beta}{\bar{t^2}}\right)^2\left\{1\pm\sqrt{1-\left(\frac{\langle d_0|\Gamma(E)|d_0\rangle\langle d_0|\Lambda(E)|d_0\rangle}{2}\right)^2}\right\}.\end{aligned} \tag{2.72}$$

This is reduced to a remarkably simple formula

$$\mathcal{G}_{\alpha\to\beta}(E) = \frac{e}{\pi}J^{\max}_{\alpha\to\beta}\left\{1\pm\sqrt{1-\left(\frac{\rho_{\mathrm{eigen}}(E)}{\rho_{\mathrm{leads}}(E)}\right)^2}\right\}, \tag{2.73}$$

where

$$\begin{cases}\rho_{\mathrm{eigen}}(E) &\equiv \dfrac{\langle d_0|\Lambda(E)|d_0\rangle}{2\pi} = \dfrac{1}{2\pi}\displaystyle\sum_n \frac{\langle d_0|\psi_n\rangle\langle\tilde{\psi}_n|d_0\rangle}{E-E_n} \\ \rho_{\mathrm{leads}}(E) &\equiv \dfrac{1}{\bar{t^2}\pi}\dfrac{\partial k_E}{\partial E} = \dfrac{1}{\bar{t^2}\pi\sqrt{4t^2-E^2}} = \dfrac{1}{\pi\langle d_0|\Gamma(E)|d_0\rangle}.\end{cases} \tag{2.74}$$

Here $\rho_{\mathrm{eigen}}(E)$ is the local density of state of the discrete eigenstates of the whole system H on the site d_0 and $\rho_{\mathrm{leads}}(E)$ is the local density of state of the lead Hamiltonians $\sum_\alpha H_\alpha$. Note that $\rho_{\mathrm{eigen}}(E)$ has singularities at the discrete eigenvalues, whereas $\rho_{\mathrm{leads}}(E)$ has singularities at the branch points. The system-independent constant

$$J^{\max}_{\alpha\to\beta} \equiv \frac{2e}{\hbar}\left(\frac{\bar{t}_\alpha\bar{t}_\beta}{\bar{t^2}}\right)^2 \tag{2.75}$$

gives the maximum possible current from the lead α to the lead β. The conductance itself has singularities due to the discrete eigenstates but not due to branch points . We exemplify $\rho_{\mathrm{eigen}}(E)$ and $\rho_{\mathrm{leads}}(E)$ in Fig. 2.8 for a two-level dot with two leads with $\bar{t}_{\alpha 1} = \bar{t}_{\alpha 2} = 1, \epsilon_0/t = 5.0, \epsilon_1/t = 0.5, v_{01}/t = 0.5$.

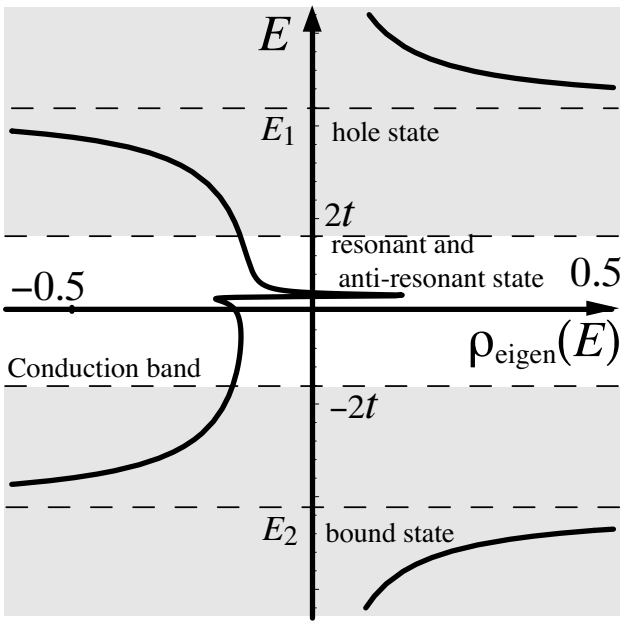

(a)

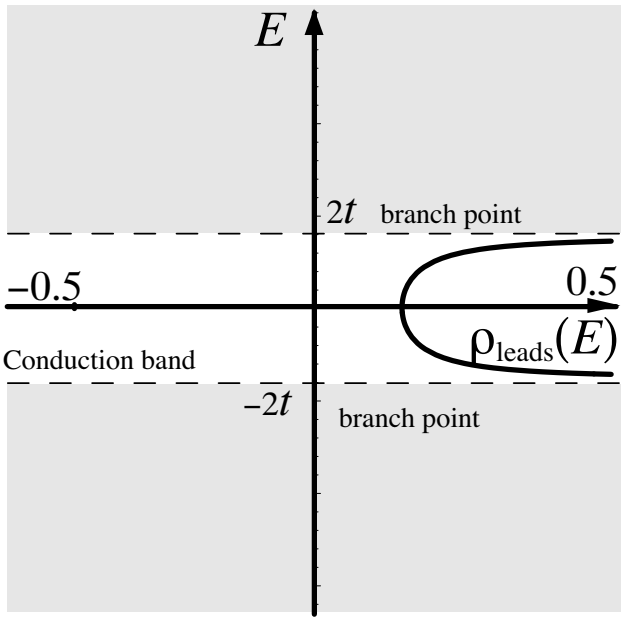

(b)

Figure 2.8: (a) The energy dependence of the local density of the states $\rho_{\text{eigen}}(E)$. (b) The energy dependence of the local density of the states $\rho_{\text{leads}}(E)$. The plots are for a two-level dot with two leads with $\bar{t}_{\alpha 1} = \bar{t}_{\alpha 2} = 1, \epsilon_0/t = 5.0, \epsilon_1/t = 0.5, v_{01}/t = 0.5$.

Chapter 3

Quantum interference effect due to the discrete eigenstates

In the present chapter, we argue that the Fano conductance arises as a result of interference between a pair of discrete eigenstates. The conductance formula (2.73) has square modulus of the local density of states of the discrete eigenstates. Therefore, we have cross terms between a pair of the resonant states as well as between a resonant state and a bound state. We show in the present chapter that discrete eigenvalues decide the symmetry of the conductance peaks in addition to the location of the conductance peaks, using several examples. We thereby describe the Fano parameter microscopically.

3.1 Point contact system

First we show the conductance and the corresponding eigenvalues of the one-level dot with two leads, namely the point contact shown in Fig. 3.1. There are only two bound states and no resonant state. We plotted in Fig. 3.2 the conductance and two bound eigenvalues for $\epsilon_0/t = 0, 1, 1.5, 2, 2.5$ with the hopping energy $\bar{t}_{\alpha_1} = \bar{t}_{\alpha_2} = 1$. The conductance of the point contact has no peculiar behavior such as the Breit-Wigner peak. Upon increasing the potential ϵ_0, the two bound eigenvalues move away from the branch points $E = \pm 2t$. This decreases the contribution of the local density of the states $\rho_{\text{eigen}}(E)$ and hence deflates the conductance gradually.

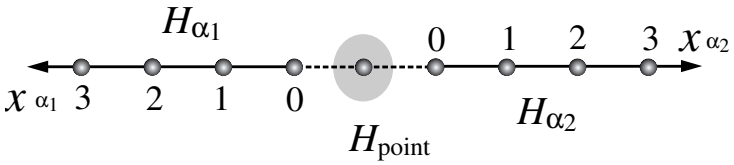

Figure 3.1: The point contact d_0 with the two leads.

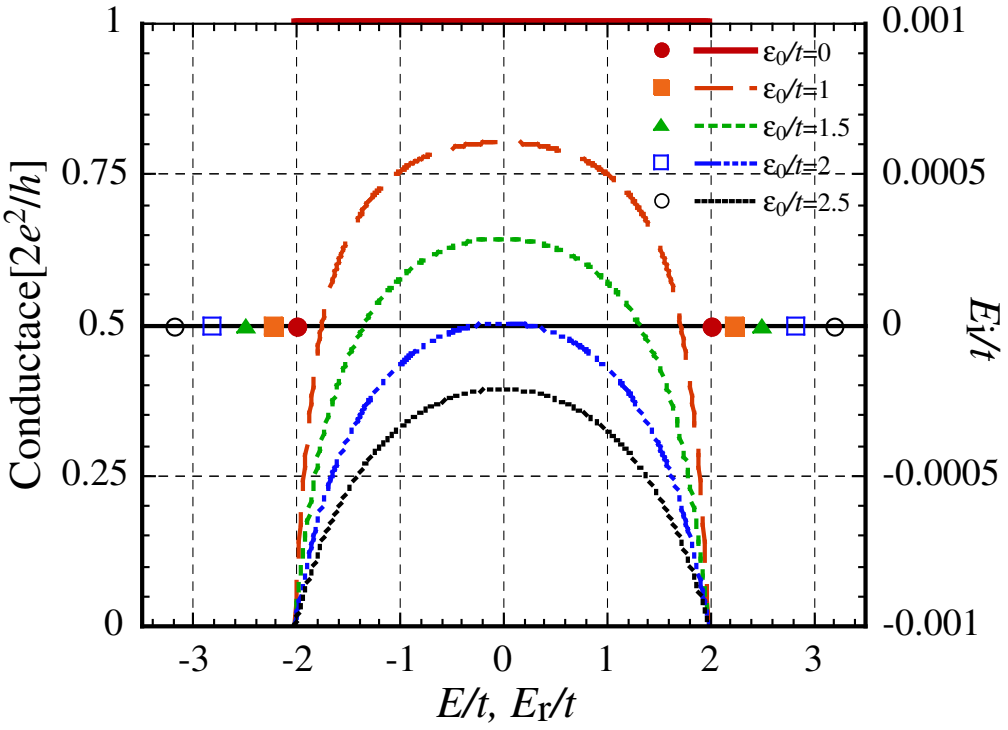

Figure 3.2: The energy dependence of the conductance (the left axis) and the discrete bound eigenvalues (the right axis).

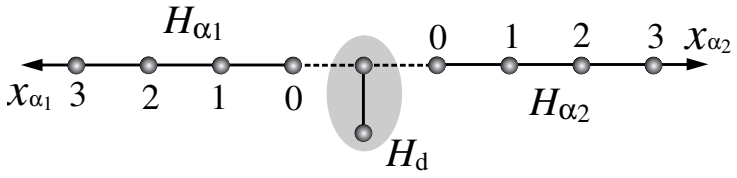

Figure 3.3: The two-level quantum dot with the two leads.

3.2 T-shaped quantum dot system

We next show that the conductance and the eigenvalues of the two-level quantum dot with two leads, namely T-shaped quantum dot shown in Fig. 3.3. This system is a minimal model that possesses a resonant state pair (a resonant state and the corresponding anti-resonant state). We obtain the conductance, two bound states and one resonant state pair for $\epsilon_0/t = 0, 1, 3, 5, \epsilon_1 = 0$ and $v_{01}/t = 1$ with $\bar{t}_{\alpha_1} = \bar{t}_{\alpha_2} = 1$ as shown in Fig. 3.4.

We have a Breit-Wigner peak for $\epsilon_0 = 0$, but for $\epsilon_0 \neq 0$, we have an asymmetric peak, namely the Fano conductance peak. Maruyama *et al.* [15] claimed that the asymmetry of the conductance peak of the T-shaped quantum dot is proportional to ϵ_0. We here discuss the asymmetry from the viewpoint of the discrete eigenstates.

We argue hereafter that the Fano conductance peak arises from the interference, or the cross term between a bound state and the resonant state pair. We compare in Fig. 3.5 the conductance formula (2.73) with the full local density of states $\rho_{\rm eigen}(E)$ and the same conductance formula but with an incomplete local density of states for $\epsilon_0/t = 5, \epsilon_1 = 0$ and $v_{01}/t = 1$ with $\bar{t}_{\alpha_1} = \bar{t}_{\alpha_2} = 1$. In Fig. 3.5 (a), we used only the two bound states as the incomplete local density of states;

$$\rho_{\rm eigen}(E) \longrightarrow \sum_{j=1,2} \rho_j(E) \equiv \sum_{j=1,2} \frac{1}{2\pi} \frac{\langle d_0|\psi_j\rangle\langle\psi_j|d_0\rangle}{E - E_j}. \tag{3.1}$$

We do not have any Breit-Wigner or Fano peaks. In Fig. 3.5 (b), on the other hand, we used only the resonant state pair as the incomplete local density of

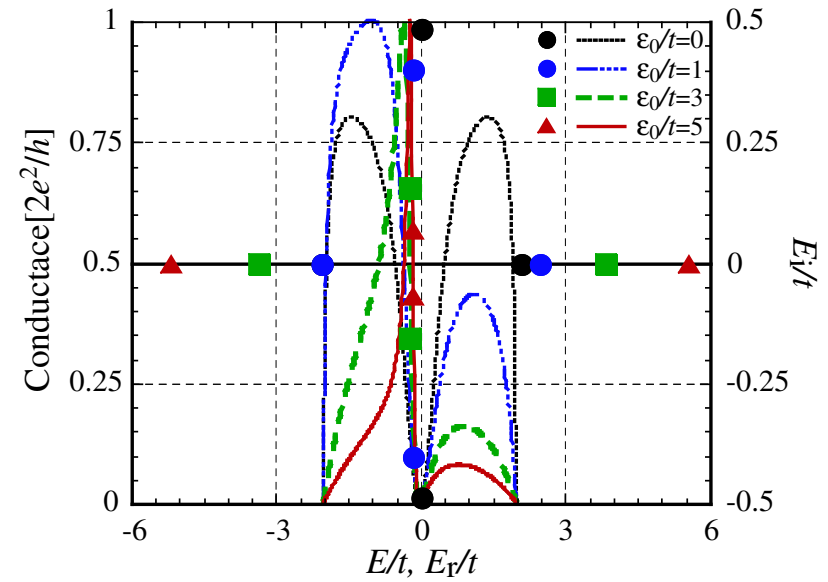

(a)

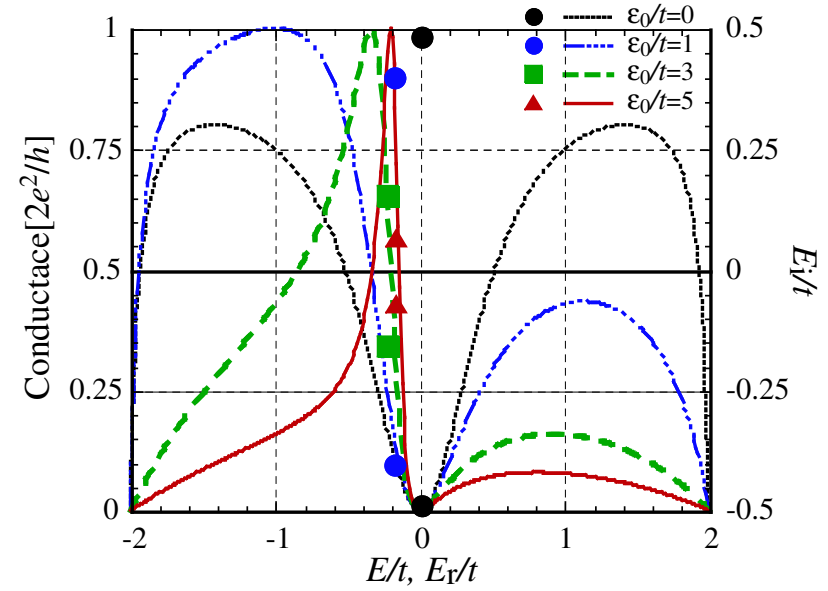

(b)

Figure 3.4: (a) The energy dependence of the conductance (the left axis) and the discrete eigenvalues (the right axis). (b) is a part of (a). Here we fixed $\epsilon_1/t = 0$ and $v_{01}/t = 1$.

states;

$$\rho_{\rm eigen}(E) \longrightarrow \rho^{\rm pair}(E) \equiv \rho^{\rm res}(E) + \rho^{\rm anti}(E) \\ \equiv \frac{1}{2\pi}\frac{\langle d_0|\psi^{\rm res}\rangle\langle\tilde{\psi}^{\rm res}|d_0\rangle}{E-E^{\rm res}} + \frac{1}{2\pi}\frac{\langle d_0|\psi^{\rm anti}\rangle\langle\tilde{\psi}^{\rm anti}|d_0\rangle}{E-E^{\rm anti}}. \tag{3.2}$$

This reproduces the asymmetry peak only partly.

We thus find that the cross term

$$\rho^{\rm pair}(E) \times \sum_{j=1,2}\rho_j(E) \tag{3.3}$$

plays the essential role. Let us approximate the cross term at the neighborhood of $E \sim E_{\rm r}^{\rm res}$ by using the normalized energy

$$\varepsilon \equiv \frac{E-E_{\rm r}^{\rm res}}{E_{\rm i}^{\rm res}}. \tag{3.4}$$

We first rewrite $\rho^{\rm res}(E)$ and $\rho^{\rm anti}(E)$ in the forms

$$\rho^{\rm res}(E) \equiv \frac{1}{2\pi}\frac{\langle d_0|\psi^{\rm res}\rangle\langle\tilde{\psi}^{\rm res}|d_0\rangle}{E-(E_{\rm r}^{\rm res}+iE_{\rm i}^{\rm res})} = \frac{|\tilde{N}|e^{i\theta}/2}{E-(E_{\rm r}^{\rm res}+iE_{\rm i}^{\rm res})} \tag{3.5}$$

$$\rho^{\rm anti}(E) \equiv (\rho^{\rm res}(E))^*, \tag{3.6}$$

where we define the coefficient of the local density of states of the resonant state as

$$|\tilde{N}|e^{i\theta} \equiv \frac{\langle d_0|\psi^{\rm res}\rangle\langle\tilde{\psi}^{\rm res}|d_0\rangle}{\pi}. \tag{3.7}$$

We then rewrite the local density of state of the resonant state pair in the form

$$\rho^{\rm pair}(E) \equiv \rho^{\rm res}(E) + \rho^{\rm anti}(E) = |\tilde{N}|\frac{(E-E_{\rm r}^{\rm res})\cos\theta + E_{\rm i}^{\rm res}\sin\theta}{(E-E_{\rm r}^{\rm res})^2 + {E_{\rm i}^{\rm res}}^2} \\ = \frac{|\tilde{N}|}{E_{\rm i}^{\rm res}}\frac{\cos\theta\varepsilon + \sin\theta}{\varepsilon^2+1}. \tag{3.8}$$

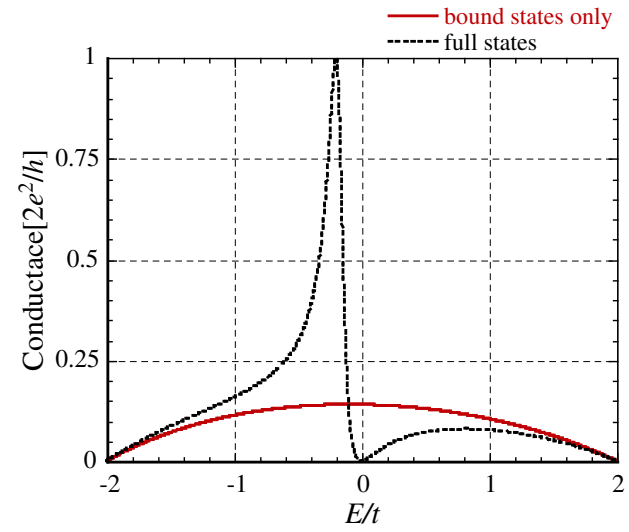

(a)

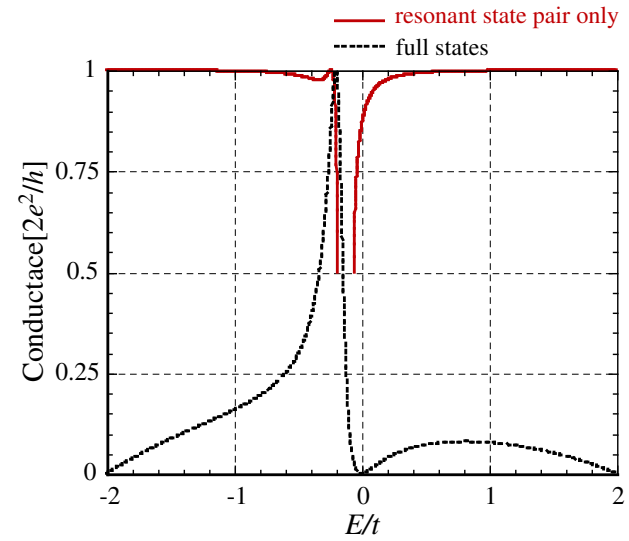

(b)

Figure 3.5: (a) The conductance with the full local density of states (the broken line) and with only the local density of two bound states (the solid line). (b) The conductance with the full local density of states (the broken line) and with only the local density of the resonant state pair (the solid line). We fixed $\epsilon_0/t = 5, \epsilon_1/t = 0$ and $v_{01}/t = 1$.

On the other hand, we approximately have the local density of states of two bound states as

$$\sum_{j=1,2} \rho_j(E) \sim \sum_{j=1,2} \left(\rho_j(E_{\rm r}^{\rm res}) + \rho_j'(E_{\rm r}^{\rm res}) E_{\rm i}^{\rm res} \varepsilon\right). \tag{3.9}$$

We therefore have the cross term between the resonant state pair and the two bound states as

$$\begin{aligned}\rho^{\rm pair}(E) \times \sum_{j=1,2} \rho_j(E) &\sim \frac{|\tilde{N}|/E_{\rm i}^{\rm res}(\cos\theta\varepsilon + \sin\theta)}{\varepsilon^2+1} \sum_{j=1,2} \left(\rho_j(E_{\rm r}^{\rm res}) + E_{\rm i}^{\rm res}\rho_j'(E_{\rm r}^{\rm res})\varepsilon\right) \\ &\sim \frac{p\varepsilon^2 + q\varepsilon + r}{\varepsilon^2+1},\end{aligned} \tag{3.10}$$

where

$$p \equiv |\tilde{N}| \cos\theta \sum_j \rho_j'(E_{\rm r}^{\rm res}), \tag{3.11}$$

$$q \equiv |\tilde{N}| \sum_j \left(\frac{\rho_j(E_{\rm r}^{\rm res})\cos\theta}{E_{\rm i}^{\rm res}} + \rho_j'(E_{\rm r}^{\rm res})\sin\theta\right), \tag{3.12}$$

$$r \equiv |\tilde{N}| \sum_j \frac{\rho_j(E_{\rm r}^{\rm res})\sin\theta}{E_{\rm i}^{\rm res}}. \tag{3.13}$$

The coefficient q of the linear term controls the asymmetry of the conductance peak. This is often referred to as the Fano parameter.

In a rather special case where $q = 0$, or $\sum_j \rho_j(E_{\rm r}^{\rm res}) = \sum_j \rho_j'(E_{\rm r}^{\rm res}) = 0$, the resonance peak takes the form of a symmetric Lorentzian. In a general case, however, we end up with an asymmetric peak. A small imaginary part $E_{\rm i}^{\rm res}$ cause a particularly large q and hence yields a particularly asymmetric peak.

For $\epsilon_0 = 0$ as shown in Fig. 3.6 (a), the conductance peak around the resonant state pair is symmetric because the bound state 1 and the bound state 2 affect the peak of the resonant state pair symmetrically. For $\epsilon_0 \neq 0$, on the other hand, the bound state 1 affects the resonant state pair more strongly than the bound state 2 does. The conductance peak around the resonant state pair is asymmetric because the bound state 1 and the bound state 2 affect the peak of the resonant state pair asymmetrically as shown in Fig. 3.6 (b).

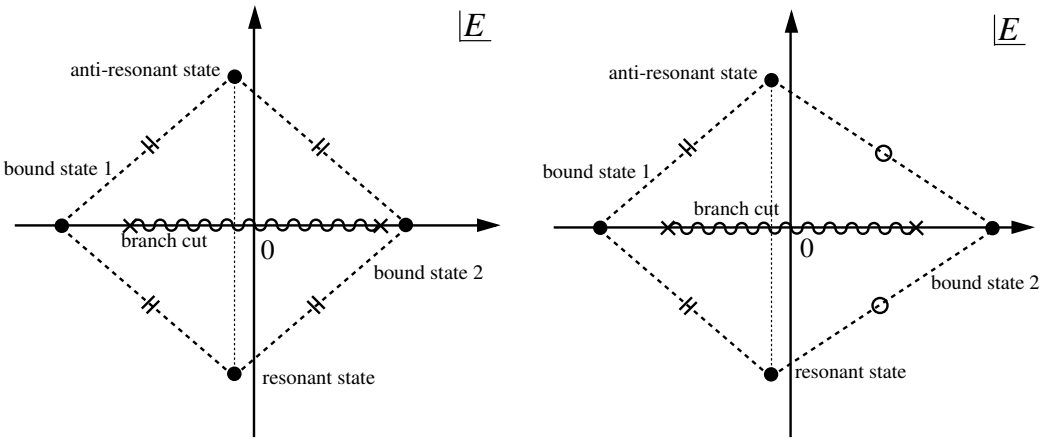

Figure 3.6: A schematic illustration of the resonant states and two bound states for (a) $\epsilon_0 = 0$ and (b) $\epsilon_0 \neq 0$.

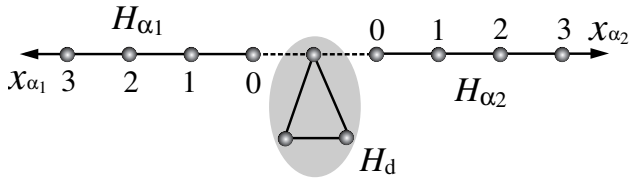

Figure 3.7: The three-level quantum dot with two leads.

3.3 Three-level quantum dot system

Third, we discuss the conductance of the three-level quantum dot with two leads shown in Fig. 3.7. This system has a possibility of yielding two resonant states. We obtain the conductance, two bound states and two resonant state pairs for $\epsilon_0/t = 0, \epsilon_1/t = -0.3, \epsilon_2/t = 0.5, v_{01}/t = 1, v_{01}/t = 0.8, v_{02}/t = 0.5$ and $v_{12}/t = 0.4$ with $\bar{t}_{\alpha_1} = \bar{t}_{\alpha_2} = 1$ as shown in Fig. 3.8.

The conductance of this system has the cross term between one resonant state pair and the other resonant state pair as well as between a resonant state pair and a bound state. The conductance formula (2.73) contains the

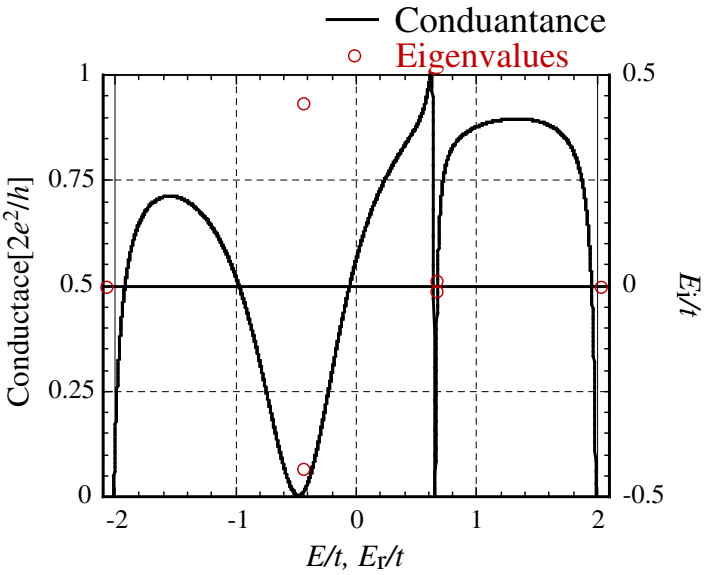

Figure 3.8: The energy dependence of the conductance (the left axis) and the eigenvalues (the right axis). We fixed $\epsilon_0/t = 0, \epsilon_1/t = -0.3, \epsilon_2/t = 0.5, v_{01}/t = 1, v_{01}/t = 0.8, v_{02}/t = 0.5$ and $v_{12}/t = 0.4$.

square of the discrete eigenvalues

$$\rho_{\rm eigen}(E) = \sum_{l=1,2} \rho_l^{\rm pair}(E) + \sum_{j=1,2} \rho_j(E) \tag{3.14}$$

with

$$\rho_l^{\rm pair}(E) \equiv |\tilde{N}_l| \frac{(E - E_{{\rm r}l}^{\rm res})\cos\theta_l + E_{{\rm i}l}^{\rm res}\sin\theta_l}{(E - E_{{\rm r}l}^{\rm res})^2 + E_{{\rm i}l}^{\rm res\,2}}. \tag{3.15}$$

Thus the conductance has the cross term between the resonant state pair 1 and the other resonant state pair 2;

$$\rho_1^{\rm pair}(E) \times \rho_2^{\rm pair}(E). \tag{3.16}$$

We approximate the cross term at the neighborhood of $E \sim E_{\rm r1}^{\rm res}$ by using the normalized energy

$$\varepsilon \equiv \frac{E - E_{\rm r1}^{\rm res}}{E_{\rm i1}^{\rm res}}. \tag{3.17}$$

We then approximately have the cross term between the resonant states pairs

$$\begin{aligned}\rho_1^{\rm pair}(E) \times \rho_2^{\rm pair}(E) &\sim \frac{|\tilde{N}_1|/E_{\rm i1}^{\rm res}(\cos\theta_1\varepsilon + \sin\theta_1)}{\varepsilon^2 + 1}\left(\rho_2^{\rm pair}(E_{\rm r1}^{\rm res}) + E_{\rm i1}^{\rm res}\rho_2^{\rm pair\prime}(E_{\rm r1}^{\rm res})\varepsilon\right) \\ &= \frac{p^{\rm res}\varepsilon^2 + q^{\rm res}\varepsilon + r^{\rm res}}{\varepsilon^2 + 1}\end{aligned} \tag{3.18}$$

with

$$p^{\rm res} \equiv |\tilde{N}_1|\cos\theta_1\rho_2^{\rm pair\prime}(E_{\rm r1}^{\rm res}), \tag{3.19}$$

$$q^{\rm res} \equiv |\tilde{N}_1|\left(\frac{\rho_2^{\rm pair}(E_{\rm r1}^{\rm res})\cos\theta_1}{E_{\rm i1}^{\rm res}} + \rho_2^{\rm pair\prime}(E_{\rm r1}^{\rm res})\sin\theta_1\right), \tag{3.20}$$

$$r^{\rm res} \equiv |\tilde{N}_1|\frac{\rho_2^{\rm pair}(E_{\rm r1}^{\rm res})\sin\theta_1}{E_{\rm i1}^{\rm res}}. \tag{3.21}$$

We thus have another Fano parameter $q^{\rm res}$ that controls the asymmetry, in addition to the coefficient q in Eq. (3.12).

In a rather special case where $q^{\rm res} = 0$, or $\rho_2^{\rm pair}(E_{\rm r1}^{\rm res}) = \rho_2^{\rm pair\prime}(E_{\rm r1}^{\rm res}) = 0$, the resonance peak takes the form of a symmetric Lorentzian. In a general

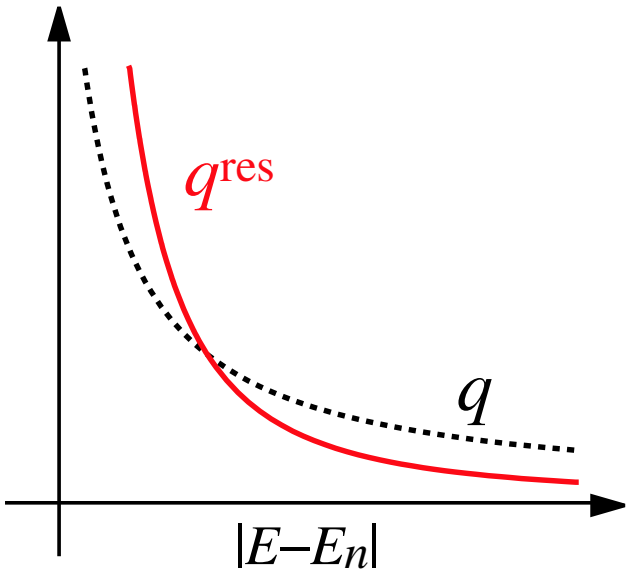

Figure 3.9: A schematic view of the decays of the Fano parameters q and q^{res}.

case, however, we end up with an asymmetric peak. A small imaginary part $E_{\mathrm{i1}}^{\mathrm{res}}$ cause a particularly large q^{res} and hence yields a particularly asymmetric peak.

Let us discuss the difference between the Fano parameters q and q^{res}. The parameter q contains $(E - E_j)^{-1}$, while the parameter q^{res} contains the Lorentzian $\left[(E - E_{\mathrm{r2}}^{\mathrm{res}})^2 + E_{\mathrm{i2}}^{\mathrm{res}2}\right]^{-1}$. When the resonant state pair 2 is quite close to the resonant state pair 1, the Lorentzian factor gets larger and makes the parameter q^{res} dominate over the parameter q. However, the Lorentzian factor decays as $\sim (E - E_{\mathrm{r2}}^{\mathrm{res}})^{-2}$ when the pair 2 moves away from the pair 1; it decays faster than the factor $(E - E_j)^{-1}$ as shown in Fig. 3.9. Then the parameter q becomes dominant.

We obtain the conductance and the discrete eigenstate for $\epsilon_0/t = 0.0, \epsilon_2/t = 0.5, v_{01}/t = 1.0, v_{01}/t = 0.8, v_{02}/t = 0.5, v_{12}/t = 0.4$ with $\bar{t}_{\alpha_1} = \bar{t}_{\alpha_2} = 1$ as shown in Fig. 3.10. Upon increasing the potential energy ϵ_1, a dipped conductance peak approaches to the other conductance peak gradually. Then the other conductance peak becomes an asymmetric peak.

We can show that the cross term between two resonant pairs forms the

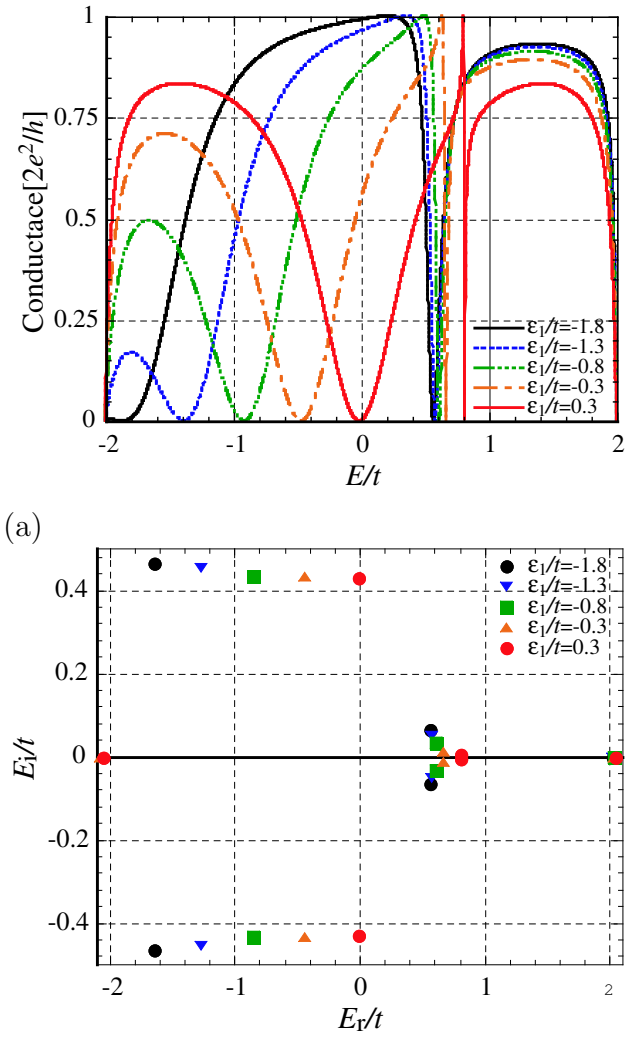

Figure 3.10: (a) The potential energy ϵ_1-dependent conductance for $\epsilon_0/t = 0.0, \epsilon_2/t = 0.5, v_{01}/t = 1.0, v_{01}/t = 0.8, v_{02}/t = 0.5, v_{12}/t = 0.4$. The dipped conductance peak of the resonant state 1 approaches the conductance peak of the resonant state 2, upon increasing the potential energy ϵ_1. Then the conductance peak of the resonant state 2 has an asymmetric peak.

Fano conductance peak. We compare in Fig. 3.11 the conductance formula (2.73) with the full local density of states $\rho_{\rm eigen}(E)$ and the same conductance formula but with an incomplete local density of states for $\epsilon_0/t = 0.0, \epsilon_2/t = 0.5, v_{01}/t = 1.0, v_{01}/t = 0.8, v_{02}/t = 0.5, v_{12}/t = 0.4$. We used only the two resonant state pair as the incomplete local density of states. This almost reproduces the asymmetry peak. We stress that the complete description of the conductance peak requires all pairs of the discrete eigenstates as shown in Fig. 3.12.

3.4 The effect of the hopping energy $\bar{t}_\alpha$ between the central dot and the leads

Finally, we discuss the effect of the hopping energy $\bar{t}_\alpha$ between the central dot and the lead α. We here deal with the case of the three-level dot with two leads case with $\bar{t}_\alpha \equiv \bar{t}_{\alpha 1} = \bar{t}_{\alpha 2}$, $\epsilon_0/t = 0.0, \epsilon_1/t = -0.3, \epsilon_2/t = 0.5, v_{01}/t = 1.0, v_{01}/t = 0.8, v_{02}/t = 0.5$ and $v_{12}/t = 0.4$. For the weakly coupled case $\bar{t}_\alpha = 0.1, 0.3$, the conductance has three sharp peaks as shown in Figs. 3.13 (a) and (b), and the system has the corresponding three resonant state pairs as shown in Fig. 3.14. Upon increasing the hopping energy $\bar{t}_\alpha$, for $\bar{t}_\alpha = 1/\sqrt{2}$ one resonant state pair collides and becomes two bound states, while the conductance continuously changes. Upon increasing further the hopping energy $\bar{t}_\alpha$, into the strongly coupled regime $\bar{t}_\alpha \geqslant 1/\sqrt{2}$, two resonant state pairs form a sharp Fano asymmetric peak.

We argue why the discrete eigenvalues have singular behavior at $\bar{t}_\alpha = 1/\sqrt{2}$. The hopping energy $\bar{t}_\alpha = 1/\sqrt{2}$ gives the sum of the squares of the hopping energy as $\bar{t^2} \equiv \sum_\alpha \bar{t}_\alpha^2 = 1$. For $\bar{t^2} = 1$, the effective potential $V_{\rm eff}(E) = -t\bar{t^2}e^{ik_E}$ discussed in Subsec. 2.2.3 cancels the term $-te^{ik_E}$ in the energy $E = -t(e^{ik_E} + e^{-ik_E})$. This changes the secular equation for the effective Hamiltonian (2.53) and causes the singular behavior of the eigenvalues.

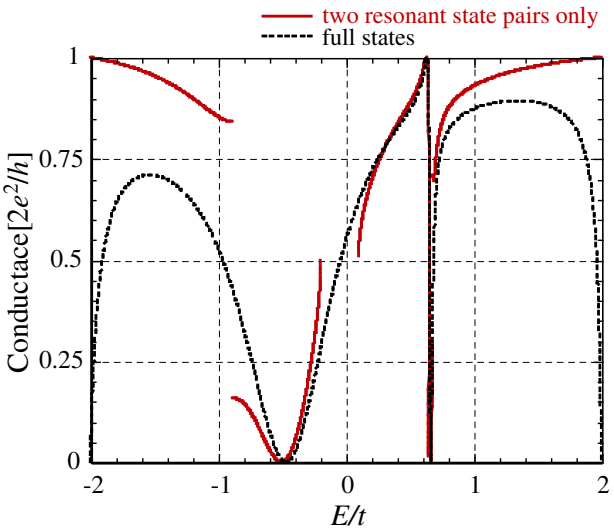

(a)

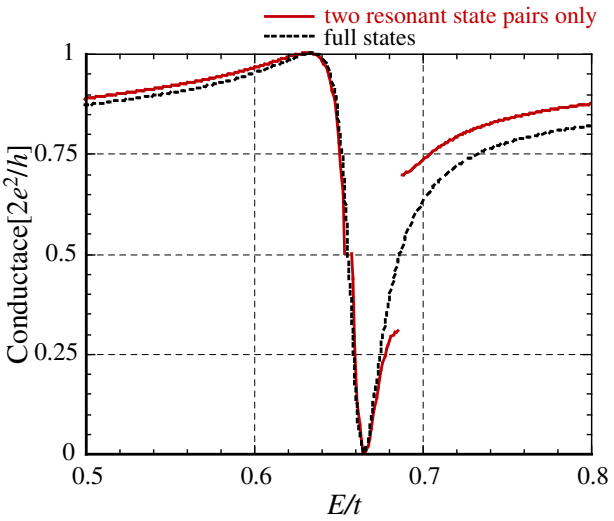

(b)

Figure 3.11: (a) The energy-dependence of the conductance with the full local density of states (the broken line) and with an incomplete local density of states for two resonant state pairs (the solid lines). (b) shows the part around $E = E_{\mathrm{r2}}^{\mathrm{res}}$.

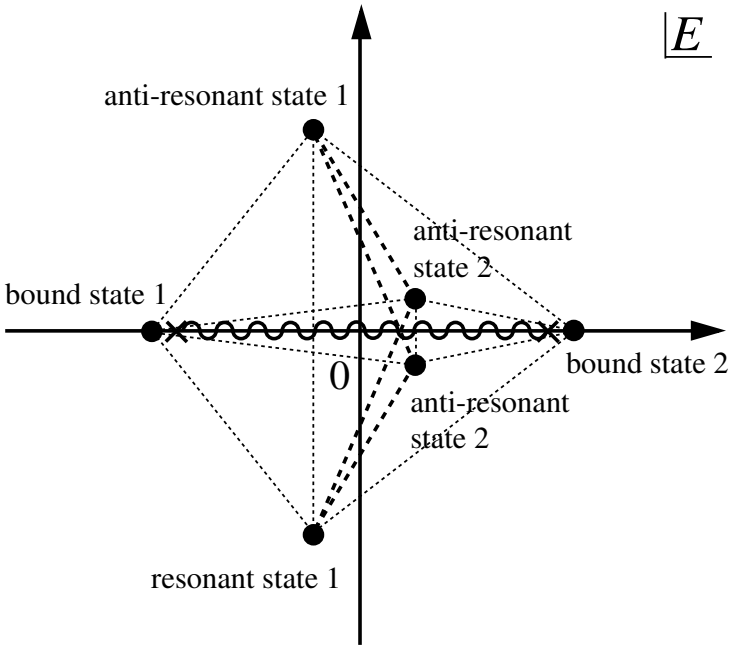

Figure 3.12: A diagrammatic illustration of the cross-terms between the discrete eigenstates of the three-level quantum dot. There is a large difference in the cross-term between the resonant state pair and resonant-bound states.

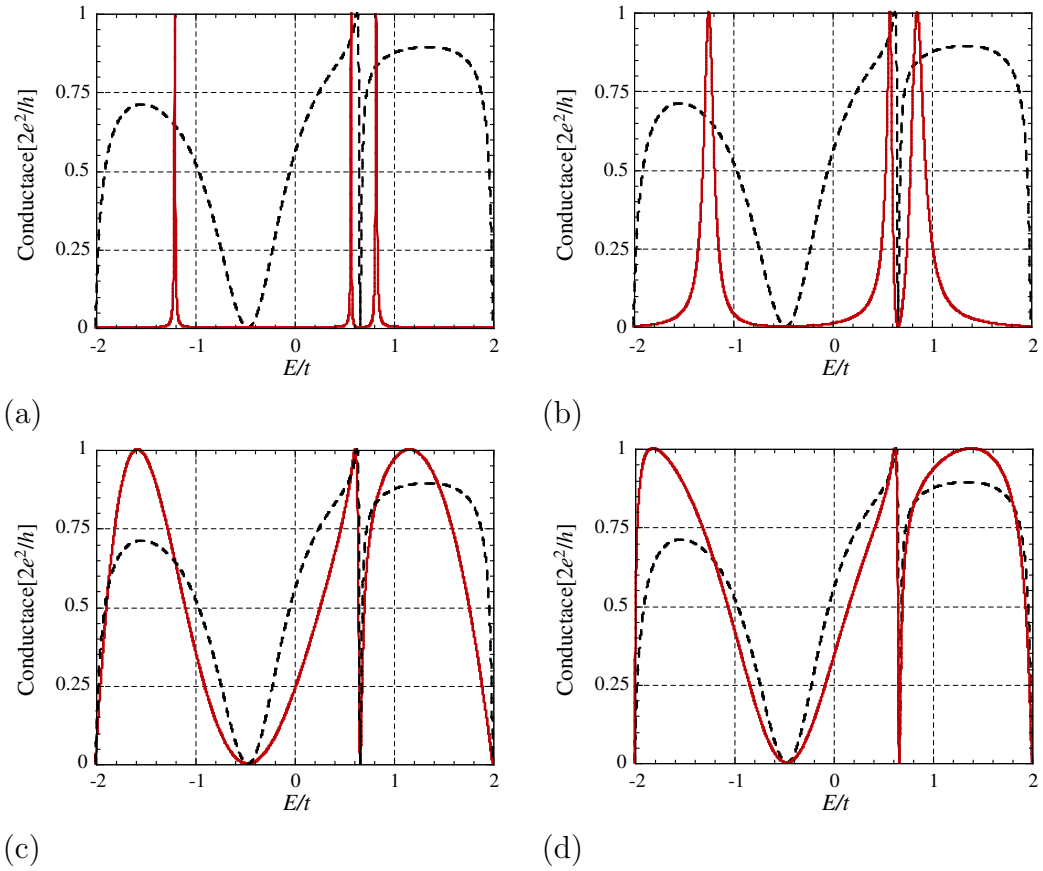

Figure 3.13: The conductance for (a) $\bar{t}_\alpha = 0.1$, (b) $\bar{t}_\alpha = 0.3$, (c) $\bar{t}_\alpha = 1/\sqrt{2}$ and (d) $\bar{t}_\alpha = 0.8$. The broken line indicates the strongly coupled case $\bar{t}_{\alpha 1} = 1$. We fixed $\epsilon_0/t = 0.0, \epsilon_1/t = -0.3, \epsilon_2/t = 0.5, v_{01}/t = 1.0, v_{01}/t = 0.8, v_{02}/t = 0.5, v_{12}/t = 0.4$.

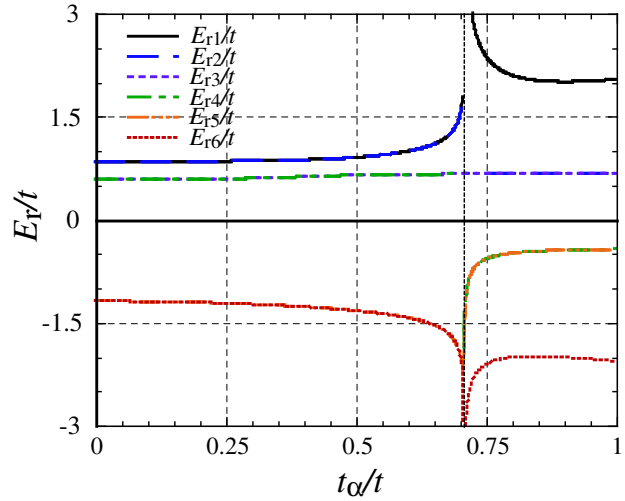

(a)

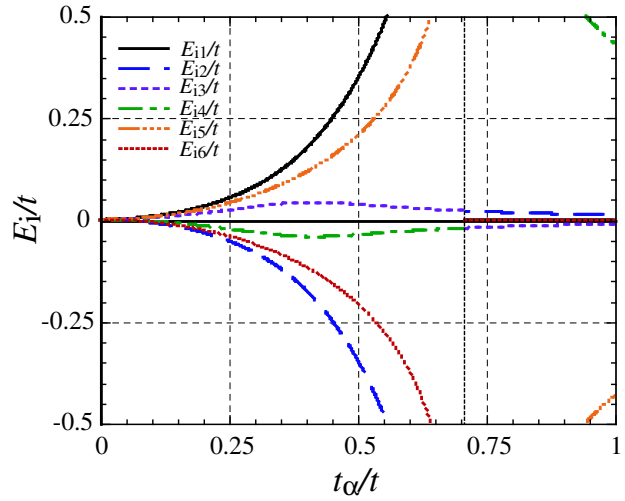

(b)

Figure 3.14: (a) The real part of eigenvalues for $\epsilon_0/t = 0.0, \epsilon_1/t = -0.3, \epsilon_2/t = 0.5, v_{01}/t = 1.0, v_{01}/t = 0.8, v_{02}/t = 0.5, v_{12}/t = 0.4$. (b) The imaginary part of eigenvalues in the same case.

Chapter 4

The conductance and the discrete eigenvalues of C_{60}

In the present chapter, we show that our discussion in the previous chapter is applicable to a general device with leads attached . We demonstrate the above method by analyzing a fullerene C_{60} (Fig. 4.1) in the form,

$$\mathcal{H}_{\rm c} = -t \sum_{\langle i,j \rangle} \left(c_i^\dagger c_j + c_j^\dagger c_i \right) \tag{4.1}$$

where t is the hopping energy between the carbon atoms. (For simplicity, we assume that the hopping energy is the same for every bond.) The leads are attached to sites of the fullerene symmetrically. The system dose not belong to the class (2.1). We show that the argument on the Fano peak still holds for the system.

Figure 4.2 shows the conductance together with the location of the resonant eigenvalue. We can clearly see that each complex eigenvalue of the resonant state corresponds to a peak of the conductance, particularly the two Fano peaks around $E_{\rm r}^{\rm res} \sim -1.65t$ and $E_{\rm r}^{\rm res} \sim 1.5t$. In other words, the Fano effect is here described by the resonant states of the whole system, not as a "coupling" of the device and the leads.

We now show that the Fano asymmetric conductance is caused by the combination of two resonant states (Fig. 4.3), one with a small imaginary part $(E_{\rm r1}^{\rm res}, E_{\rm i1}^{\rm res})$ and one with a large imaginary part $(E_{\rm r2}^{\rm res}, E_{\rm i2}^{\rm res})$ under the relation $E_{\rm i1}^{\rm res} < |E_{\rm r1}^{\rm res} - E_{\rm r2}^{\rm res}| < E_{\rm i2}^{\rm res}$. The denominator of the conductance near the resonance $E_1^{\rm res} = E_{\rm r1}^{\rm res} + iE_{\rm i1}^{\rm res}$ takes the form $|E - E_1^{\rm res}|^2 = (E - E_{\rm r1}^{\rm res})^2 + E_{\rm i1}^{\rm res 2}$,

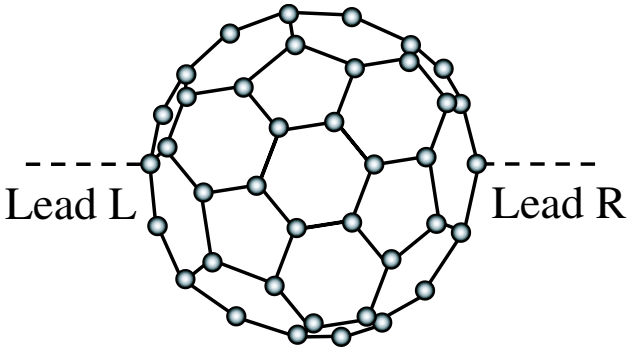

Figure 4.1: A fullerene C_{60} with two leads attached.

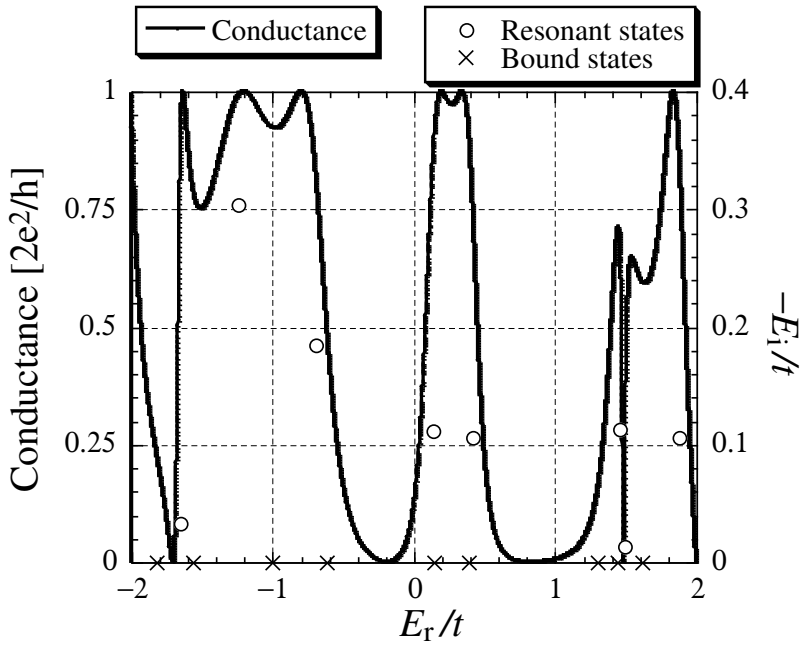

Figure 4.2: The energy dependence of the conductance (the left axis) of the fullerene in Fig. 4.1 and its resonant eigenvalues (the right axis). The circles denote resonant eigenvalues and the symbols × denote bound states. The resonant eigenvalues obtained from the advanced Green's function are omitted, because they are complex conjugate to the retarded ones.

and hence we would expect a sharp Lorentzian peak. However, the numerator of the conductance also has the energy dependence because of the nearby broad conductance peak at $E \simeq E_{\rm r2}^{\rm res}$:

$$T(E) \simeq \frac{\rho_2(E)}{\left(E - E_{\rm r1}^{\rm res}\right)^2 + E_{\rm i1}^{\rm res\,2}} \tag{4.2}$$

with

$$\rho_2(E) \simeq \frac{1}{\left(E - E_{\rm r2}^{\rm res}\right)^2 + E_{\rm i2}^{\rm res\,2}}. \tag{4.3}$$

This can be written in the form

$$T(\varepsilon) \simeq \frac{r^{\rm res} + q^{\rm res}\varepsilon}{\varepsilon^2 + 1} \tag{4.4}$$

with $\varepsilon \equiv (E - E_{\rm r1}^{\rm res})/E_{\rm i1}^{\rm res}$ and $r^{\rm res} \equiv \rho_2(E_{\rm r1}^{\rm res})/E_{\rm i1}^{\rm res\,2}$. We define the normalized asymmetry coefficient, or the Fano parameter as

$$q^{\rm res} \equiv \rho_2'(E_{\rm r1}^{\rm res})/E_{\rm i1}^{\rm res}. \tag{4.5}$$

This is roughly equal to Eq. (3.20).

In a rather special case where $q^{\rm res} = 0$, or $\rho_2'(E_{\rm r1}^{\rm res}) = 0$, the resonance peak takes the form of a symmetric Lorentzian. In a general case, however, we end up with an asymmetric peak. A resonant state with a small imaginary part $E_{\rm i1}^{\rm res}$ has a particularly large $q^{\rm res}$ and hence yields a particularly asymmetric peak. From this viewpoint, the asymmetric Fano peak is a surprisingly general phenomenon.

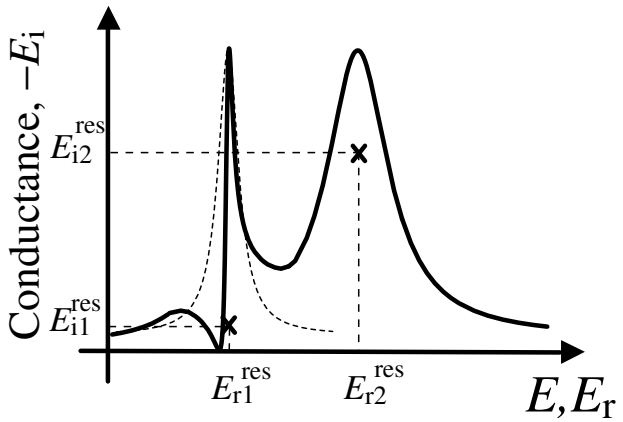

Figure 4.3: The Fano conductance (the curves) together with the location of the resonant eigenvalues (the crosses).

Chapter 5

Summary

We carried out the spectrum analysis of the open quantum N-level dot with the multiple leads. We obtain the conductance formula in terms of the discrete eigenstates, containing the resonant, anti-resonant and bound states, as well as the branch points. In Chap. 2, we showed that the resonant state generally has a diverging eigenfunction and a complex eigenvalue. We reduced the Hamiltonian of an infinite system to the effective one of a finite system, using the self-energy. We obtain the simple conductance formula (2.73) by using the local density of states of discrete eigenstates, $\rho_{\rm eigen}(E)$, and the local density of states of the leads, $\rho_{\rm leads}(E)$. In Chap. 3, we showed that the Fano conductance arises from the cross terms between two resonant state pairs as well as a resonant state pair and a bound state. We also presented microscopic derivation of the Fano parameter. In Chap. 4, we showed calculation of the conductance of a C_{60} molecule. The conductance has a complicated structure but the shapes of the peaks can be essentially described by the argument in Chap. 3.

Appendix A: The scattering state obtained by the Lippmann-Schwinger equation

In this appendix, we present in detail the calculation of the expression of the scattering states given in Eq. (2.11)[19]. First, for simplicity, we transform the Hamiltonian of Eq.(2.1) to the second-quantized Hamiltonian

$$\hat{\mathcal{H}} = \hat{\mathcal{H}}_0 + \hat{\mathcal{H}}_1 \tag{5.1}$$

$$\hat{\mathcal{H}}_0 \equiv \sum_{\alpha} \int_{-\pi}^{\pi} \frac{dk}{2\pi} E_k \psi^{\dagger}_{k,\alpha} \psi_{k,\alpha} + \sum_{j=0}^{N-1} \epsilon_j d_j^{\dagger} d_j \tag{5.2}$$

$$\hat{\mathcal{H}}_1 \equiv -\sum_{\alpha} t_{\alpha} \int_{-\pi}^{\pi} \frac{dk}{2\pi} \left(\psi^{\dagger}_{k,\alpha} d_0 + \text{h.c.} \right) - \sum_{0 \leqslant i < j \leqslant N-1} \left(v_{ij} d_i^{\dagger} d_j + \text{h.c.} \right). \tag{5.3}$$

where $\psi^{\dagger}_{k,\alpha}$ and $\psi_{k,\alpha}$ are the Fermion field operators of the lead α while $d_j^{\dagger}$ and d_j are the creation and annihilation operators of the Fermion, respectively. These operators obey the anticommutation relations;

$$\left\{ \psi^{\dagger}_{k,\alpha}, \psi_{k',\alpha'} \right\} = \delta_{k,k'} \delta_{\alpha\alpha'} \quad \text{and} \quad \left\{ d_i^{\dagger}, d_j \right\} = \delta_{i,j}, \tag{5.4}$$

$$\{ \psi_{k,\alpha}, \psi_{k',\alpha'} \} = 0 \quad \text{and} \quad \{ d_i, d_j \} = 0. \tag{5.5}$$

We next define the Hamiltonians are assigned a Liouville operators $\mathcal{L}_0$ and $\mathcal{L}_1$, which act on a general operator $\hat{\mathcal{O}} \in \left\{ \psi^{\dagger}_{k,\alpha}, \psi_{k,\alpha}, d_j^{\dagger}, d_j \right\}$ as

$$\mathcal{L}_n \hat{\mathcal{O}} \equiv \left[\hat{\mathcal{O}}, \hat{\mathcal{H}}_n \right] \quad \text{for } n = 0, 1, \tag{5.6}$$

where $[\cdot,\cdot]$ is the commutation relation. The Liouville operator $\mathcal{L}$ for the Hamiltonian $\hat{\mathcal{H}}$ of the whole system is given by

$$\mathcal{L} \equiv \left[\hat{\mathcal{O}}, \hat{\mathcal{H}}\right] = \left[\hat{\mathcal{O}}, \hat{\mathcal{H}}_0 + \hat{\mathcal{H}}_1\right] = \left[\hat{\mathcal{O}}, \hat{\mathcal{H}}_0\right] + \left[\hat{\mathcal{O}}, \hat{\mathcal{H}}_1\right] = \mathcal{L}_0 + \mathcal{L}_1. \tag{5.7}$$

Third, we define the scattering-state operators $c^\dagger_{k,\alpha}$ and $c_{k,\alpha}$ of the lead α, which have the anti-commutation relations

$$\left\{c^\dagger_{k,\alpha}, c_{k',\alpha'}\right\} = \delta_{k,k'}\delta_{\alpha\alpha'} \quad \text{and} \quad \{c_{k,\alpha}, c_{k',\alpha'}\} = 0. \tag{5.8}$$

These scattering-state operator have the outgoing wave boundary condition as follows;

$$\mathcal{L}c^\dagger_{k,\alpha} = \left[c^\dagger_{k,\alpha}, \hat{\mathcal{H}}\right] = -E_k c^\dagger_{k,\alpha} + i\delta\left(\psi^\dagger_{k,\alpha} - c^\dagger_{k,\alpha}\right), \tag{5.9}$$

where δ is a positive infinitesimal. Equation (5.9) is rewritten as

$$c^\dagger_{k,\alpha} = \frac{i\delta}{\mathcal{L} + E_k + i\delta}\psi^\dagger_{k,\alpha}. \tag{5.10}$$

We express the scattering-state operator $c^\dagger_{k,\alpha}$ in terms of the known operators $\psi^\dagger_{k,\alpha}, d^\dagger_j$

$$c^\dagger_{k,\alpha} = \psi^\dagger_{k,\alpha} - \frac{1}{\mathcal{L} + E_k + i\delta}\mathcal{L}_1\psi^\dagger_{k,\alpha}as \tag{5.11}$$

by using the relation among $\mathcal{L}$ and $\mathcal{L}_0, \mathcal{L}_1$,

$$\frac{1}{\mathcal{L} + E_k + i\delta} = \left\{1 - \frac{1}{\mathcal{L} + E_k + i\delta}\mathcal{L}_1\right\}\frac{1}{\mathcal{L}_0 + E_k + i\delta} \tag{5.12}$$

with

$$\frac{1}{\mathcal{L}_0 + E_k + i\delta}\psi^\dagger_{k,\alpha} = \frac{1}{i\delta}\psi^\dagger_{k,\alpha}. \tag{5.13}$$

Finally, we calculate the scattering-state operator $c^\dagger_{k,\alpha}$. Defining the operators

$$\hat{D}_j \equiv \frac{1}{\mathcal{L} + E_k + i\delta}d^\dagger_j, \tag{5.14}$$

$$\hat{F}_{q,\alpha} \equiv \frac{1}{\mathcal{L} + E_k + i\delta}\psi^\dagger_{q,\alpha}, \tag{5.15}$$

we simplify the scattering-state operator by using the relation

$$c^\dagger_{k,\alpha} = \psi^\dagger_{k,\alpha} - t_\alpha \hat{D}_0, \tag{5.16}$$

where

$$\begin{aligned}
\hat{D}_0 &= \left\{1 - \frac{1}{\mathcal{L} + E_k + i\delta}\mathcal{L}_1\right\} \frac{1}{\mathcal{L}_0 + E_k + i\delta} d^\dagger_0 \\
&= \frac{1}{E_k - \epsilon_0 + i\delta}\left(d^\dagger_0 - \sum_{j=1}^{N-1} v_{0j}\hat{D}_j - \sum_\beta t_\beta \int_{-\pi}^{\pi} \frac{dq}{2\pi}\hat{F}_{q,\beta}\right), \qquad (5.17) \\
\hat{D}_j &= \left\{1 - \frac{1}{\mathcal{L} + E_k + i\delta}\mathcal{L}_1\right\} \frac{1}{\mathcal{L}_0 + E_k + i\delta} d^\dagger_j \\
&= \frac{1}{E_k - \epsilon_j + i\delta}\left(d^\dagger_j - \sum_{l=j+1}^{N-1} v_{jl}\hat{D}_l - \sum_{l=0}^{j-1} v^*_{lj}\hat{D}_l\right), \qquad (5.18) \\
\hat{F}_{q,\beta} &= \left\{1 - \frac{1}{\mathcal{L} + E_k + i\delta}\mathcal{L}_1\right\} \frac{1}{\mathcal{L}_0 + E_k + i\delta}\psi^\dagger_{q,\beta} = \frac{1}{E_k - E_q + i\delta}\left(\psi^\dagger_{q,\beta} - t_\beta \hat{D}_0\right). \qquad (5.19)
\end{aligned}$$

Using Eqs. (5.17) and (5.19), we can obtain a matrix equation

$$\begin{pmatrix}
E_k - \epsilon_0 + i\delta - \sum_\alpha \int_{-\pi}^{\pi} \frac{dq}{2\pi} \frac{t^2_\alpha}{E_k - E_q + i\delta} & v_{01} & \cdots & v_{0,N-1} \\
v^*_{01} & E_k - \epsilon_1 + i\delta & \cdots & v_{1,N-1} \\
\vdots & \vdots & \ddots & \vdots \\
v^*_{0,N-1} & v^*_{1,N-1} & \cdots & E_k - \epsilon_{N-1} + i\delta
\end{pmatrix}$$
$$\times \begin{pmatrix} \hat{D}_0 \\ \hat{D}_1 \\ \vdots \\ \hat{D}_{N-1} \end{pmatrix} = \begin{pmatrix} d^\dagger_0 - \sum_\beta \int_{-\pi}^{\pi} \frac{dq}{2\pi} \frac{t_\beta \psi^\dagger_{q,\beta}}{E_k - E_q + i\delta} \\ d^\dagger_1 \\ \vdots \\ d^\dagger_N \end{pmatrix}. \tag{5.20}$$

On the other hand, using the inverse of the retarded Green's function of

Eq. (2.49)

$$\begin{aligned}
&\left(G^R(E_k)\right)^{-1} = E_k - H_{\rm eff}(E_k) \\
&= \begin{pmatrix}
E_k - \epsilon_0 + i\delta - \sum_\alpha \int_{-\pi}^{\pi} \frac{dq}{2\pi} \frac{t_\alpha^2}{E_k - E_q + i\delta} & v_{01}^* & \cdots & v_{0,N-1}^* \\
v_{01} & E_k - \epsilon_1 + i\delta & \cdots & v_{1,N-1}^* \\
\vdots & \vdots & \ddots & \vdots \\
v_{0,N-1} & v_{1,N-1} & \cdots & E_k - \epsilon_{N-1} + i\delta
\end{pmatrix},
\end{aligned} \tag{5.21}$$

we obtain

$$\begin{pmatrix} \hat{D}_0 \\ \hat{D}_1 \\ \vdots \\ \hat{D}_{N-1} \end{pmatrix} = \left(G^{\rm R}(E_k)\right)^t \begin{pmatrix} d_0^\dagger - \sum_\beta \int_{-\pi}^{\pi} \frac{dq}{2\pi} \frac{t_\beta \psi_{q,\beta}^\dagger}{E_k - E_q + i\delta} \\ d_1^\dagger \\ \vdots \\ d_{N-1}^\dagger \end{pmatrix} \tag{5.22}$$

We write the scattering-state operator of the lead α as

$$c_{k,\alpha}^\dagger = \psi_{k,\alpha}^\dagger - t_\alpha \left(\sum_{j=0}^{N-1} d_j^\dagger d_j - \sum_\beta \int_{-\pi}^{\pi} \frac{dq}{2\pi} \frac{t_\beta \psi_{q,\beta}^\dagger}{E_k - E_q + i\delta} d_0 \right) G^{\rm R}(E_k) d_0^\dagger. \tag{5.23}$$

The scattering states in the first-quantized form is thereby given as

$$\begin{aligned}
|\psi_{k,\alpha}^{\rm F}\rangle &\equiv c_{k,\alpha}^\dagger |0\rangle \\
&= |k,\alpha\rangle - t_\alpha \left(\sum_{j=0}^{N-1} \langle d_j | G^{\rm R}(E_k) | d_0 \rangle | d_j \rangle - \langle d_0 | G^{\rm R}(E_k) | d_0 \rangle \sum_\beta \int_{-\pi}^{\pi} \frac{dq}{2\pi} \frac{t_\beta |q,\beta\rangle}{E_k - E_q + i\delta} \right).
\end{aligned} \tag{5.24}$$

Appendix B:Calculation of the self-energy due to the outgoing-wave boundary condition

A popular way of treating the semi-infinite leads is to contract the leads to the self-energy. The self-energy of leads is a useful way of computing the conductance as well as obtaining resonant states. In this Appendix, we propose a new method of calculating the self-energy of the leads. The self-energy $\Sigma(E)$ was originally defined in [1]

$$\langle x|\frac{1}{E-H+i\delta}|x'\rangle = \langle x|\frac{1}{E-(H_c+\Sigma(E))}|x'\rangle \tag{5.25}$$

for sites x and x' inside the central conductor, where H_c is the Hamiltonian of the central conductor and H is the total Hamiltonian including semi-infinite leads attached to the conductor. The self-energy has been calculated by various methods. The method that we present here is much easier than previous methods. The main claim of this note is that the self-energy is equivalent to the boundary conditions for resonant states.

We consider the Hamiltonian of a conductor with semi-infinite leads attached to it: $H = H_c + \sum_\alpha H_\alpha$, where H_c is a one-body Hamiltonian of a finite-size conductor, while H_α describes a semi-infinite lead given by the tight-binding model

$$H_\alpha \equiv -t\sum_{x_\alpha=0}^{\infty}(|x_\alpha+1\rangle\langle x_\alpha| + |x_\alpha\rangle\langle x_\alpha+1|). \tag{5.26}$$

This includes the hopping between a site $x_\alpha = 0$ on the conductor and the lead α. (Note that, if we have hopping between the conductor and a lead with the amplitude different from $-t$, we include it in H_c.)

Equation (5.25) suggests that the eigenvalues of the effective Hamiltonian $H_{\text{eff}}(E) \equiv H_c + \Sigma(E)$ are the poles (bound states and resonant states) of the total Hamiltonian H on the complex E plane. Therefore, we seek discrete and generally complex eigenvalues E_n of resonant states and bound states of the whole system:

$$H|\psi_n\rangle = E_n|\psi_n\rangle \quad \text{and} \quad \langle\tilde{\psi}_n|H = E_n\langle\tilde{\psi}_n|. \tag{5.27}$$

The eigenfunctions are bi-orthogonal: $\langle\tilde{\psi}_n|\psi_m\rangle = \delta_{nm}$. The eigenvalues E_n are related to the corresponding eigen-wave-number k_n, which is also generally complex, through the dispersion relation $E_n = -2t\cos k_n$. The eigen-wave-number k_n is on the upper-half plane for the bound states and on the lower-half plane for the resonant states.

It is known that the resonant states as well as the bound states can be found by requiring the boundary conditions $\langle x_\alpha|\psi_n\rangle \propto e^{ik_n x_\alpha}$ for $x_\alpha \geq 0$ in the leads[11]. In other words, the discrete states satisfy the boundary conditions

$$\langle x_\alpha + 1|\psi_n\rangle = e^{ik_n}\langle x_\alpha|\psi_n\rangle \quad \text{for } x_\alpha \geq 0, \tag{5.28}$$

where $\Re k_n \geq 0$. The boundary conditions transform the Schrödinger equation

$$\langle x_\alpha = 0|H_c|\psi_n\rangle - t\langle x_\alpha = 1|\psi_n\rangle = E_n\langle x_\alpha = 0|\psi_n\rangle \tag{5.29}$$

to

$$\begin{aligned}\langle x_\alpha = 0|H_c|\psi_n\rangle + V_{\text{eff}}^{(\alpha)}(E_n)\langle x_\alpha = 0|\psi_n\rangle \\ = E_n\langle x_\alpha = 0|\psi_n\rangle,\end{aligned} \tag{5.30}$$

where

$$V_{\text{eff}}^{(\alpha)}(E) \equiv -te^{ik} \tag{5.31}$$

is the energy-dependent effective potential.

We claim that the self-energy of the lead α is nothing but the effective potential:

$$\Sigma^{(\alpha)}(E) = V_{\text{eff}}^{(\alpha)}(E)|x_\alpha = 0\rangle\langle x_\alpha = 0|. \tag{5.32}$$

The total self-energy is the sum over the leads: $\Sigma(E) = \sum_{\alpha} \Sigma^{(\alpha)}(E)$. The effective potential $V_{\rm eff}^{(\alpha)}$ is rewritten in terms of E as

$$V_{\rm eff}^{(\alpha)}(E) \equiv \frac{E - i\sqrt{4t^2 - E^2}}{2} \tag{5.33}$$

by using the dispersion relation $E = -2t\cos k$. Note that we choose the branch $\Im V_{\rm eff}^{(\alpha)} < 0$ for the retarded Green's function. Equation (5.33) is indeed equivalent to the expression obtained by other methods[1].

Let us now demonstrate that the present method is easily generalized to other types of leads such as N-leg ladder and carbon nanotube. Hereafter, we drop the lead index α for simplicity. First, we calculate the self-energy of a lead of N-leg ladder (Fig.5.1):

$$\begin{aligned} H_{\rm ladder} = & -t\sum_{x=0}^{\infty}\sum_{y=1}^{N}\left(|x+1,y\rangle\langle x,y|\right. \\ & \left. +|x,y+1\rangle\langle x,y| + \text{c.c.}\right). \end{aligned} \tag{5.34}$$

We first diagonalize $H_{\rm ladder}$ in the y direction and obtain the conduction channels $\{\phi_j(y)\,|j = 1, 2, \cdots, N\}$, where

$$\phi_j(y) = \sin\frac{j\pi y}{N+1}\Big/\sqrt{\sum_{y''=1}^{N}\sin^2\frac{j\pi y''}{N+1}}. \tag{5.35}$$

Each channel has the dispersion relation $E = -2t\cos k_j + \omega_j$, where $\omega_j \equiv -2t\cos(2\pi j/N)$. Each channel yields its effective potential of the form Eq. (5.31), or

$$V_{\rm eff}^{(j)}(E) = -te^{ik_j} = \frac{E - \omega_j - i\sqrt{4t^2 - (E-\omega_j)^2}}{2}. \tag{5.36}$$

The self-energy of N-leg ladder is given in the $N \times N$ matrix form

$$\left(\Sigma_{\rm ladder}(E)\right)_{y,y'} = \sum_{j=1}^{N}\phi_j(y)V_{\rm eff}^{(j)}(E)\phi_j(y')^*. \tag{5.37}$$

The result is equivalent to the one obtained in Ref. [16].

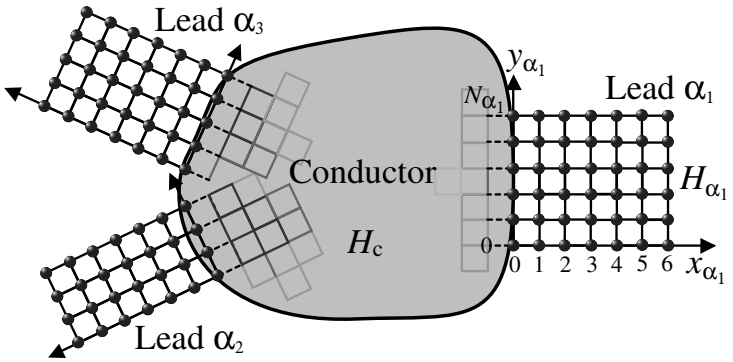

Figure 5.1: Leads of the form of ladders are attached to the central conductor.

Second, we calculate the self-energy of a lead of (n,0) zigzag carbon nanotube attached to the conductor as in Fig. 5.2, where n is the chiral number. The Schrödinger equation of the zigzag carbon nanotube $H_{\rm zigzag}|\psi^{\pm}_{\rm A/B}(k_j)\rangle = E|\psi^{\pm}_{\rm A/B}(k_j)\rangle$ yields the dispersion relation of the jth channel as

$$E = \pm t\left|h_{k_j}\right| = \pm t\sqrt{1 \pm 4\cos\frac{\sqrt{3}k_j}{2}\cos\frac{\pi j}{n} + 4\cos^2\frac{\pi j}{n}}, \tag{5.38}$$

with

$$h_{k_j} \equiv e^{i\frac{k_j}{\sqrt{3}}} + 2\cos\frac{\pi j}{n}e^{-i\frac{k_j}{2\sqrt{3}}} \tag{5.39}$$

where the first Brillouin zone is $|k_j| < \pi/\sqrt{3}$ [17], and its wavefunction on the A and B sub-lattices as

$$\begin{cases} \langle x, y|\psi^{\pm}_{\rm A}(k_j)\rangle = & \mp\dfrac{h^*_{k_j}}{|h_{k_j}|}e^{ik_j x}\phi_j(y), \\ \langle x, y|\psi^{\pm}_{\rm B}(k_j)\rangle = & e^{ik_j x}\phi_j(y), \end{cases} \tag{5.40}$$

where $\phi_j(y) \equiv e^{i\frac{2\pi j}{n}y}/\sqrt{n}$. The boundary conditions transform the Schrödinger equation of the whole system

$$\begin{aligned} \langle x = 0, y|H_c|\psi^{\pm}_{\rm B}(k_j)\rangle - t\langle x = 1/\sqrt{3}, y|\psi^{\pm}_{\rm A}(k_j)\rangle \\ = E\langle x = 0, y|\psi^{\pm}_{\rm B}(k_j)\rangle \end{aligned} \tag{5.41}$$

to

$$\begin{aligned}\langle x=0,y|H_c|\psi^{\pm}_{\rm B}(k_j)\rangle + V^{(j;B)}_{\rm zigzag}(E)\langle x=0,y|\psi^{\pm}_{\rm B}(k_j)\rangle \\ =E\langle x=0,y|\psi^{\pm}_{\rm B}(k_j)\rangle,\end{aligned} \tag{5.42}$$

where the effective potential of the jth channel is given by

$$V^{(j;B)}_{\rm zigzag}(E) \equiv \pm t\frac{h^*_{k_j}}{|h_{k_j}|}e^{i\frac{k_j}{\sqrt{3}}} \tag{5.43}$$

$$= \frac{E^2+t^2-\lambda_j^2 \pm i\sqrt{(2t\lambda_j)^2-\left(E^2-t^2-\lambda_j^2\right)^2}}{2E} \tag{5.44}$$

with $\lambda_j \equiv 2t\cos\pi j/n$. Hence we obtain the self-energy of an (n,0) carbon nanotube in the $n\times n$ matrix form

$$\left(\Sigma_{\rm zigzag}(E)\right)_{y_{\rm B},y'_{\rm B}} = \sum_{j=1}^{n}\phi_j(y_{\rm B})V^{(j;B)}_{\rm zigzag}(E)\phi_j(y'_{\rm B})^*, \tag{5.45}$$

where $y_{\rm A}$ and $y_{\rm B}$ are coordinates on the A and B sub-lattices, respectively, which are indicated in Fig. 5.2. The result (5.45) is indeed equivalent to the one obtained in Ref. [18].

When the A sub-lattice, instead of the B sub-lattice, is in contact with the conductor, we obtain the self-energy in the form

$$\left(\Sigma_{\rm zigzag}(E)\right)_{y_{\rm A},y'_{\rm A}} = \sum_{j=1}^{n}\phi_j(y_{\rm A})V^{(j;A)}_{\rm zigzag}(E)\phi_j(y'_{\rm A})^* \tag{5.46}$$

with

$$\begin{aligned}&V^{(j;A)}_{\rm zigzag}(E)\\ \equiv&\frac{E^2-t^2+\lambda_j^2 \pm i\sqrt{(2t\lambda_j)^2-\left(E^2-t^2-\lambda_j^2\right)^2}}{2E}.\end{aligned} \tag{5.47}$$

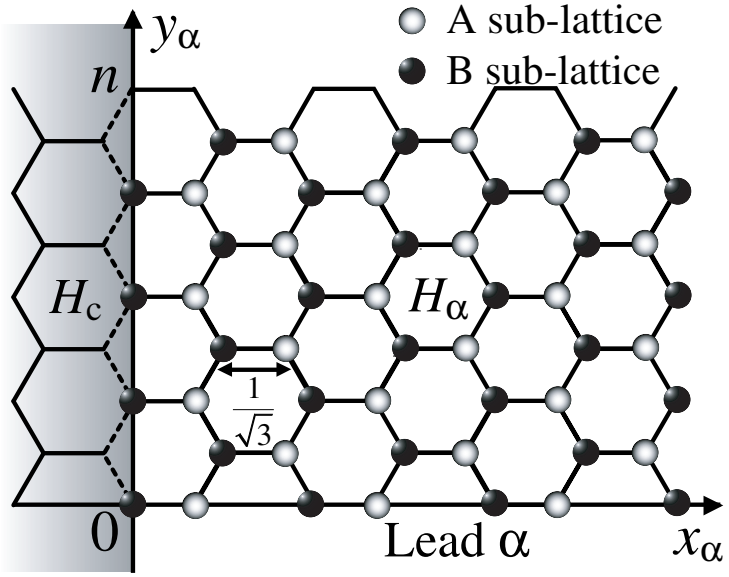

Figure 5.2: A lead of the zigzag carbon nanotube. The upper and lower edges satisfy the periodic boundary conditions.

Bibliography

[1] *e.g.* S. Datta, *Electronic Transport in Mesoscopic Systems* (Cambridge University Press, Cambridge, 1995).

[2] U. Fano, Phys. Rev. **124** (1961) 1866.

[3] K. Kobayashi, H. Aikawa, S. Katsumoto, and Y. Iye, Phys. Rev. Lett. **88** (2002) 256806.

[4] K. Kobayashi, H. Aikawa, S. Katsumoto, and Y. Iye, Phys. Rev. B **68** (2003) 235304.

[5] K. Sasada and N. Hatano, Physica E **29** (2005) 609.

[6] K. O. Friedrichs, Commun. Pure Appl. Math. **1** (1948) 361

[7] T. Petrosky, I. Prigogine and S. Tasaki, Physica A **173** (1991) 175.

[8] G. Ordonez, T. Petrosky and I. Prigogine, Phys. Rev. A **63** (2001) 052106.

[9] M. Miyamoto, Phys. Rev. A **72** (2005) 063405.

[10] R. G. Newton, *Scattering Theory of Waves and Particles, 2nd edition* (Springer-Verlag, New York, 1982).

[11] N. Hatano, K. Sasada, H. Nakamura and T. Petrosky: avXiv:0705.1388, submitted to Prog. Theor. Phys.

[12] Ya. B. Zel'dovich, Sov. Phys. JETP **12** (1961) 542.

[13] K. Sasada and N. Hatano, J. Phys. Soc. Japan **77** (2008) to appear.

[14] D. S. Fisher and P. A. Lee, Phys. Rev. B **23** (1981) 6851.

[15] I. Maruyama, N. Shibata and K. Ueda, J. Phys. Soc. Japan **73** (2004) 3239.

[16] I. Appelbaum, T. Wang, J. D. Joannopoulos and V. Narayanamurti, Phys. Rev. B **69** (2004) 165301.

[17] R. Saito, M. Fujita, G. Dresselhaus, and M. S. Dresselhaus, Phys. Rev. B **46** (1992) 1804; Appl. Phys. Lett. **60** (1992) 2204.

[18] J. Guo, S. Datta, M. Lundstrom, and M. P. Anantram, Int. J. Mult. Comp. Eng. **2** (2004) 257.

[19] A. Schiller and S. Hershfield, Phys. Rev. B **58** (1998) 14978.